A Pvr–AP-1–Mmp1 signaling pathway is activated in astrocytes upon traumatic brain injury

Tingting Li[1], Wenwen Shi[1], Margaret S. Ho[2,3,*], Yong Q. Zhang[1,*]

[1]Key Laboratory of Molecular and Developmental Biology, Institute of Genetics and Developmental Biology, University of Chinese Academy of Sciences, Chinese Academy of Sciences, Beijing 100101, China.

[2]Institute of Neuroscience, National Yang Ming Chiao Tung University, Taipei, Taiwan

[3]Brain Research Center, National Yang Ming Chiao Tung University, Taipei, Taiwan

*Correspondence: margaret.ho@nycu.edu.tw, yqzhang@genetics.ac.cn (lead contact)

Main Points:

- The study provided RNA-seq data of astrocytes following traumatic brain injury (TBI)
- Genes involved in endocytic trafficking are upregulated in astrocytes after TBI
- A new Pvr–AP-1–Mmp1 pathway is activated in astrocytes following TBI.
- Inhibition of endocytosis in astrocytes upregulates the Pvr–AP-1–Mmp1 signaling.

Abstract

Traumatic brain injury (TBI) caused by external mechanical forces is a major health burden worldwide, but the underlying mechanism in glia remains largely unclear. We report herein that *Drosophila* adults exhibit a defective blood-brain-barrier (BBB), elevated innate immune responses, and astrocyte swelling upon consecutive strikes with a high-impact trauma device. RNA sequencing (RNA-seq) analysis of these astrocytes revealed upregulated expression of genes encoding PDGF and VEGF receptor-related (Pvr, a receptor tyrosine kinase (RTK)), adaptor protein complex 1 (AP-1, a transcription factor complex of the c-Jun N-terminal Kinase (JNK) pathway) composed of Jun-related antigen (Jra) and kayak (kay), and matrix metalloproteinase 1 (Mmp1) following TBI. Interestingly, Pvr is both required and sufficient for AP-1 and Mmp1 upregulation, while knockdown of AP-1 expression in the background of Pvr overexpression in astrocytes rescued Mmp1 upregulation upon TBI, indicating that Pvr acts as the upstream receptor for the downstream AP-1–Mmp1 transduction. Moreover, dynamin-associated endocytosis was found to be an important regulatory step in downregulating Pvr signaling. Our results identify a new Pvr–AP-1–Mmp1 signaling pathway in astrocytes in response to TBI, providing potential targets for developing new therapeutic strategies of TBI.

Keywords: TBI, astrocytes, Pvr, RNA-seq, *Drosophila*

52 ## Introduction

53 Traumatic brain injury (TBI) is one of the leading causes for adult disability due
54 to limited neurological recovery (Joy et al., 2019). About 43% of people discharged
55 after hospitalization for acute TBI develop long-term locomotor disability (Ma et al.,
56 2014). TBI triggers primary neural injuries via rapid physical forces that damage
57 axons, glia and blood vessels (Chodobski et al., 2011; Daneshvar et al., 2015),
58 followed by diverse secondary damage such as Wallerian axon degeneration (Büki
59 and Povlishock, 2006) and blood-brain barrier (BBB) dysfunction (Chodobski et al.,
60 2011) in the central nervous system (CNS). The outcome of TBI is affected by various
61 factors including age and diet (Byrns et al., 2021; Katzenberger et al., 2016). In
62 addition, glial cells are critical mediators in response to TBI in the mammalian brain
63 (Mira et al., 2021). During TBI, astrocytes become active, a process characterized by
64 swelling, scar tissue formation, and engulfment of neuronal debris (Liddelow et al.,
65 2017; Sofroniew and Vinters, 2010), while microglia rapidly transform to their active
66 state to phagocytose cell debris (Davalos et al., 2005).

67 *Drosophila melanogaster* is an ideal model organism for discovering new gene
68 networks and investigating the molecular and cellular responses to CNS injury (Ayaz
69 et al., 2008; Bier, 2005; Hoopfer et al., 2006; MacDonald et al., 2006). *Drosophila*
70 astrocyte-like glia (henceforth astrocytes), the conserved counterparts for mammalian
71 astrocytes, and ensheathing glia (ENG) constitute the major glial subclasses in the
72 CNS (Doherty et al., 2009; Stork et al., 2014). A previous study revealed that
73 *Drosophila* ENG perform the phagocytic function by the engulfment receptor Draper
74 which interacts with downstream signaling components, including ced-6, Shark,
75 Src42a, c-Jun N-terminal Kinase (JNK), and Mmp1 in the glial engulfment process in
76 response to axotomy (Awasaki et al., 2006; Doherty et al., 2014; Lu et al., 2014; Lu et
77 al., 2017; Purice et al., 2017). Although ENG function upon axotomy has been well
78 characterized, the response of other types of glia such as astrocytes to neural injury
79 remains unclear.

80 In mammals, signaling by platelet-derived growth factor (PDGF) directs cell
81 migration, alters cell shape, and plays a role in wound healing (Hoch and Soriano,
82 2003; Sil et al., 2018). Meanwhile, vascular endothelial growth factor (VEGF)
83 signaling is critical for cell proliferation and survival, and vascular endothelial cell
84 mitogenesis and permeability (Apte et al., 2019; Sakurai et al., 2005). Pvr, short for
85 PDGF- and VEGF receptor-related, is the sole *Drosophila* ortholog of the PDGF and
86 VEGF receptor families (Cho et al., 2002). Pvr interacts with different signaling
87 molecules in a context-dependent manner. For example, Pvr regulates thorax closure
88 during metamorphosis via the c-Jun N-terminal Kinase (JNK) signaling pathway
89 (Ishimaru et al., 2004), but the Pvr-mediated wound-induced epidermal cell migration
90 does not depend on JNK (Wu et al., 2009). The JNK/Activator Protein-1 (AP-1)
91 signaling pathway is involved in different cellular processes, including cell migration
92 (Pastor-Pareja et al., 2004), organ size control (Willsey et al., 2016), and cell death
93 (Moreno et al., 2002). The JNK effector AP-1 complex, composed of heterodimeric
94 Jun/Jun-related antigen (Jra) and Fos/kayak (kay), promotes transcription of genes
95 including matrix metalloproteinase 1 (Mmp1) that functions in tissue remodeling,
96 regulation of inflammatory processes, and metastasis of cancer cells (Egeblad and
97 Werb, 2002; Page-McCaw et al., 2007; Parks et al., 2004).
98 Previous studies have implicated a role for ensheathing glia, Draper pathway,
99 and the innate immune pathway in response to TBI (Doherty et al., 2009; Lu et al.,
100 2017; Purice et al., 2017; Katzenberger et al., 2013). However, whether astrocytes
101 also play a role in TBI response remains elusive. Herein, using a *Drosophila* TBI
102 model induced with a high-impact trauma (HIT) device (Katzenberger et al., 2013),
103 we found that TBI caused multiple defects including upregulated expression of innate
104 immune genes and astrocyte swelling. To uncover the molecular pathways activated
105 by TBI, we performed RNA sequencing (RNA-seq) analysis of astrocytes sorted by
106 fluorescence-activated cell sorting (FACS) to profile TBI-induced genes. Interestingly,
107 we showed that the expression of Pvr, AP-1, and Mmp1 was upregulated following

108 TBI. Knockdown of Pvr or AP-1 expression in astrocytes rescued TBI-induced Mmp1
109 upregulation, while Pvr overexpression promoted Mmp1 expression via AP-1 upon
110 TBI. Our findings identify a new Pvr–AP-1–Mmp1 signaling pathway that acts
111 predominantly in astrocytes in response to TBI, and shed light on the mechanisms of
112 astrocyte responses following TBI.
113

114 ## Materials and Methods:

115 ### *Drosophila* stocks and husbandry

116 Flies were maintained on standard cornmeal medium at 25°C otherwise indicated.
117 The following *Drosophila* strains were used: w^{1118}, *UAS-mCD8::GFP*, *R86E01-Gal4*
118 (#45914; Bloomington), *R54F03-Gal4* (#39157; Bloomington), *UAS-Redstinger*
119 (#8547; Bloomington), *UAS-Jra* (#7216; Bloomington), *UAS-kay* (#7213;
120 Bloomington), *UAS-Pvr* (#58429; Bloomington), *UAS-nLacZ* (#3955, Bloomington),
121 *PCNA-GFP* (#25749; Bloomington) (Thacker et al., 2003), and *TRE-dsRed*
122 (Chatterjee and Bohmann, 2012). *UAS-draper-RNAi*, *UAS-Pvr-RNAi*, *UAS-Jra-RNAi*,
123 *UAS-kay-RNAi*, *UAS-Arpc2-RNAi*, *UAS-cpa-RNAi*, *UAS-cpb-RNAi*, *UAS-Stam-RNAi*,
124 *UAS-Vps24-RNAi*, and *UAS-Chmp1-RNAi* flies were obtained from Tsinghua Fly
125 Center (https://thfc.zzbd.org/en). *yw UAS-CD8::GFP hs-FLP; tubP-Gal80*
126 *FRT-40A/CyO; alrm-Gal4 UAS-CD8::GFP UAS-Dcr2/TM6 Tb Hu* (alrm-Gal4 is a
127 specific driver in astrocytes (Doherty et al., 2009), a gift from Oren Schuldiner) and
128 *FRT-40A* (a gift from Liqun Luo) were used for MARCM analysis of astrocytes.
129 *UAS-shibire*^{ts1} (Pfeiffer et al., 2012) was provided by Y. Zhong at Tsinghua University.
130

131 ### Traumatic brain injury (TBI) Assay

132 Construction and use of the HIT device were described previously (Katzenberger
133 et al., 2013). Deflection of the spring to 90° was the standard angle for strike.
134 Mortality index at 24 h (MI_{24}) were determined by analyzing at least 120 flies (20 flies
135 for each test).

136

137 **Dye penetration assay**

138 Dye penetration experiments were performed as previously described (Bainton et
139 al., 2005). 10 kD Texas red-conjugated dextran (Molecular Probes) at 2.5 mM was
140 injected into the soft tissue between two abdominal segments of the exoskeleton of
141 flies with and without TBI. Flies were allowed to recover in fresh food tubes and
142 photographed 2 h later on a Zeiss microscope to detect the integrity of brain-eye
143 barrier (BEB). To detect the integrity of BBB, fly brains were dissected at 2 h after
144 injection and examined under an Olympus FluoView FV1000 microscope.

145

146 **MARCM analysis**

147 Mosaic analysis with a repressible cell marker (MARCM) analysis in astrocytes
148 was carried out largely following previous publications (Jia et al., 2019; Lee and Luo,
149 1999). Specifically, newly laid eggs were collected for a 4–5 h interval and cultured at
150 18°C. Clones were induced by heat shock at 24 h after larval hatching in a 37°C water
151 bath for 15 min and flies were raised at 25°C after heat shock until
152 immunohistochemistry analysis of adult brain.

153

154 **Immunohistochemistry analysis and confocal microscopy**

155 Brain tissues were dissected out from adult after specific treatments. Fixation and
156 staining of adult brains were performed as previously described (Jia et al., 2019).
157 Brains were mounted on slides in Vectashield mounting media (Vector Labs). Primary
158 antibodies were used at the following dilutions: chicken anti-GFP (ab13970, Abcam)
159 at 1:1000, mouse anti-Repo (8D12, DSHB) at 1:100, mouse anti-Elav (9F8A9, DSHB)
160 at 1:100, mouse anti-Mmp1 (3A6B4, 3B8D12, and 5H7B11, DSHB) each at 1:20 for
161 all three antibodies, rabbit anti-Pvr (McDonald et al., 2003) at 1:1000, rabbit
162 anti-Dcp-1 (Asp216, Cell Signaling Technology (CST)) at 1:100, rabbit anti-pH3
163 (06-570, Millipore) at 1:1000, and mouse anti-β-gal (40-1a, DSHB) at 1:100. All

secondary antibodies (Alexa Fluor 488, 568 or 633 labeled; Molecular Probes) were used at a dilution of 1:1000. The nuclei dye To-Pro-3 Iodide (T3605, ThermoFisher) was also used at a dilution of 1:1000. The cell-permeant Mitotracker (M22426, ThermoFisher) was used at a concentration of 100 nM. For soma diameter analysis, we measured the average of long and short axes of astrocytes. All images were collected using an Olympus FV1000 laser scanning confocal microscope and processed with ImageJ. Serial images of 25–30 μm (one image per 1 μm slice) were projected for presentation and statistical analysis.

Astrocyte preparation for RNA-seq analysis

Flies were collected at 3 days after eclosion and treated with TBI. Brains from adult flies (*R86E01-Gal4*/*UAS-Redstinger*) with no injury, 4 h after injury and 24 h after injury were dissected out in freshly prepared adult hemolymph saline (AHS) buffer, as previously described (Yang et al., 2016). Briefly, a total of ~50 brains for each group was immediately transferred to an Eppendorf tube (1.5 mL) containing 200 μL AHS with Pronase (1 mg/mL; P5147, SigmaAldrich) and Dispase (1 mg/mL; LS02104, Worthington Biochemical Corporation). After tissue digestion for 30 min at 25°C, the enzyme medium was removed, followed by two brief, gentle washes with fresh AHS containing 2% PBS. Brain samples were then triturated by gently pipetting in 1 mL AHS through four fire-polished Pasteur pipettes with descending pore sizes (400 μm, 300 μm, 200 μm, and 100 μm) for a total of ~20 min. Next, the dissociated cells were centrifuged for 10 min at 100 × *g* and the AHS was replaced with the same buffer to minimize any RNA content released from damaged cells during the trituration process. Finally, dissociated tissues were filtered through 45 μm filter and then put on ice. FACS sorting was performed according to the following gating procedure with 70 μm nozzle by BD FACS Aria: (1) an initial SSC-A/FSC-A gate to minimize debris; (2) a SSC-A/pe-Texa Ted-A gate to choose only red fluorescence positive cells. At this step, 1600 cells were sorted directly into ice-cold cell lysis

192 buffer (oligo-dT_{30}VN primer, ribonuclease inhibitor, dNTP mix) and stored at −80°C
193 until all samples were ready for RNA extraction and cDNA amplification.
194
195 **cDNA library preparation**
196 A total of 5 biological replicates were collected for each condition (no injury, 4 h
197 after injury, and 24 h after injury). Cell samples were sent to the Anoroad Company
198 for RNA extraction. An Oligo-dT primer was introduced to the reverse transcription
199 reaction for first-strand cDNA synthesis, followed by PCR amplification to enrich the
200 cDNA and magbeads purification step was used to purify the products. Briefly,
201 Smart-Seq2 method was used to amplify cDNA. Concentration and integrity of cDNA
202 was assessed using Qubit 3.0 Flurometer (Life Technologies) and Agilent 2100
203 Bioanalyzer (Agilent Technologies) to ensure the cDNA length was around 1-2 kbp.
204 After quality control, 40 ng cDNA was used to be fragmented at 350 bp by
205 Bioruptor® Sonication System (Diagenode Inc.). To construct Illumina library, end
206 repair, 3' ends A-tailing, adaptor ligation, PCR amplification and library validation
207 were performed. PerkinElmer LabChip® GX Touch and Step OnePlus™ Real-Time
208 PCR System were used for library quality inspection. Qualified libraries were loaded
209 on Illumina Hiseq platform for PE150 sequencing.
210
211 **RNA-seq and data analysis.**
212 A total of 539 million reads (average 35.9 million reads per sample) was obtained.
213 The fastq data were first processed with Trimmomatic (Bolger et al., 2014) to remove
214 Illumina adaptor. The remaining data was aligned against the UCSC *D. melanogaster*
215 genome (dm6) using Hisat2 (Kim et al., 2015; Kim et al., 2019; Pertea et al., 2016)
216 with the annotation file of the same version. On average, 92% of the initial reads were
217 mapped to dm6. HTSeq was used to calculate the raw read counts of genes for each
218 sample. DESeq2 (Love et al., 2014) was used to normalize the data. Transcripts were
219 considered as significantly differentially expressed if their adjusted *p* values were less

220 than 0.01 ($p < 0.01$) by the Benjamini-Hochberg method. Following normalization of
221 the data, DESeq2 was used to perform pairwise comparisons between the control and
222 experimental groups using parametric tests. Genes with absolute value of logarithmic
223 fold change ($\log_2$FC) > 1.0 were qualified for the final set of DEGs. Volcano plots and
224 heatmap were constructed for visualization of the resulting expression intensity data
225 following the identification of DEGs and RNA-Seq data normalization by the
226 adjusted *p* value calculations.
227
228 **Quantitative reverse transcription-PCR analysis**
229 RT-qPCR was performed largely based on previous protocols (Zhao et al., 2020).
230 Flies were treated with the same conditions as the RNA-seq experiment. RNA for
231 antimicrobial peptides (AMPs) analysis was extracted from whole fly brains by TriZol.
232 RNA for confirming RNA-seq findings was isolated from more than 10000 astrocytes
233 sorted by FACS using the PicoPure RNA isolation kit (KIT0204, Life Technologies).
234 cDNA was generated with SuperScript III First-Strand Synthesis SuperMix
235 (11752250, Invitrogen). For each gene, at least three pairs of qPCR primers were
236 screened by standard curve analysis, and the best primer pairs were chosen based on
237 their efficiency and specificity. Real-time qPCR was carried out by KAPA Library
238 Quantification Kit (KR0389, KAPA Biosystems). Primer sequences are provided in
239 Table S1.
240
241 **Thermogenetic inhibition of endocytosis**
242 For inhibition of endocytosis in astrocytes using *UAS-Shi*^{ts}, crosses were reared
243 and treated by HIT device at 23°C to avoid unintended inactivation. For
244 thermogenetic inactivation, flies after TBI were undergone intermittent temperature
245 treatment at 32°C (32°C for 30 min, and then back to 23°C for 30 min, for four
246 rounds, four hours in total) until dissection.
247

248 **Statistical analysis**

249 All statistical comparisons were performed using GraphPad Prism software, with
250 significance indicated by ∗∗∗ ($p \leq 0.001$), ∗∗ ($p \leq 0.01$), ∗ ($p \leq 0.05$), and ns ($p > 0.05$).
251 One-way ANOVA was used to compare multiple group means. Student's t-tests were
252 used for statistical comparisons between two groups.

253

254 ## Results

255 **TBI is induced in *Drosophila* adults by a high-impact trauma (HIT) device**

256 To analyze how brains respond to TBI, we applied consecutive strikes to adult
257 flies using a HIT device to induce brain injury as described previously (Katzenberger
258 et al., 2015). To quantify the degree of injury, we analyzed the mortality index at 24 h
259 after TBI (MI_{24}), defined as the percentage of dead over the total flies tested.
260 Consistent with a previous report (Katzenberger et al., 2013), MI_{24} of 3-day-old adult
261 flies was 20 ± 3.18% after 4 HIT strikes (Figure 1A). MI_{24} after 6 strikes was 71.88 ±
262 7.44%, suggesting that increasing the number of strikes results in a higher MI_{24} rate
263 (Figure 1A). Given that TBI has been shown to disrupt the formation of the
264 blood-brain barrier (BBB) in mammals and flies and blood-eye barrier (BEB) in flies
265 (Rodríguez-Baeza et al., 2003; Sangiorgi et al., 2013; Katzenberger et al., 2015;
266 Saikumar et al., 2020), we examined BBB/BEB integrity 2 h after injecting
267 tetramethylrhodamine-conjugated dextran (molecular weight = 10,000 Da) into adult
268 fly abdominal segments (Bainton et al., 2005). The dye crossed the barrier and
269 penetrated the retina and brain, indicating that both BBB and BEB were disrupted
270 after HIT strikes (Figures 1B – G). The percentage of flies exhibiting
271 dextran-permeable BBB increased as the number of strikes increased from 0 to 6, with
272 six strikes resulting in severe BBB disruption (Figure 1G) but maintaining a moderate
273 viability providing enough samples for phenotypic analysis. Based on these results,
274 six HIT strikes administered at 5 min intervals were applied to induce TBI throughout
275 the present study.

276 In addition to disruption of BBB/BEB integrity, we also analyzed TBI-induced
277 secondary damage such as local and systemic immune responses. Given that Toll and
278 immune deficiency (Imd) are the two crucial innate immune response pathways in
279 *Drosophila* (Valanne et al., 2011), and their common downstream genes encode
280 antimicrobial peptides (AMPs) that protect flies from TBI injury (Alphen et al., 2022),
281 we analyzed the expression of AMPs in adult fly brains at different time points after
282 TBI. As shown by the real-time reverse transcriptase-polymerase chain reaction
283 (RT-qPCR) results, expression of the AMP genes *AttC*, *DiptB* and *Mtk* was
284 significantly upregulated at 1 h and reached a peak at 4 h after injury (Figure 1H),
285 consistent with previous reports (Barekat et al., 2016; Katzenberger et al., 2013).
286 Taken together, these results suggest that HIT strikes induce TBI reflected by
287 BBB/BEB disruption and elevated expression of innate immune response genes.
288
289 **TBI induces neuronal but not glial apoptosis in adult fly brains**
290 Given that neurons and glia have been shown to undergo cell death during both
291 primary and secondary injury responses upon TBI in humans (Ng and Lee, 2019), we
292 performed immunostaining with an antibody against Death caspase-1 (Dcp-1), the
293 homolog of human caspase-3, to detect apoptotic cells in our TBI model. Interestingly,
294 the number of Dcp-1^{+} puncta was significantly increased in adult fly brains at 24 h
295 after TBI (Figures 1I and J), with a 2.47-fold increase compared to the number in
296 uninjured controls (Figure 1K). Furthermore, we found that almost all Dcp-1^{+} puncta
297 were co-localized with Elav rather than Repo, suggesting that neurons but not glia are
298 apoptotic (Figures 1L – M"). These results suggest that, as in mammals, TBI also
299 induces neuronal apoptosis in fruit flies.
300
301 **TBI leads to astrocyte activation**
302 In addition to the TBI-induced neuronal apoptosis mentioned above, glial cells
303 also become reactive after nervous system injury (Burda and Sofroniew, 2014). It has

304 been shown that ENG phagocytose neuronal debris upon axotomy (Doherty et al.,
305 2009), but whether astrocytes respond to TBI remains unknown. To explore the
306 potential role of astrocytes in the TBI response, *R86E01-GAL4* (Kremer et al., 2017),
307 an astrocyte-specific driver, was used to express *UAS-mCD8::GFP* to label astrocyte
308 plasma membrane. In uninjured fly brains, GFP intensities in the cell bodies and
309 processes of astrocytes were widely distributed throughout the brain (Figures 2A and
310 2D). While no significant change in GFP intensity was detected in brains at 4 h after
311 TBI (Figures 2B and 2D), the GFP intensity was significantly increased and the cell
312 bodies of astrocytes were significantly enlarged at 24 h after TBI in the central brain
313 region, especially in the antennal lobes (ALs) (Figures 2C and 2D). Of note, these
314 results were not affected by the presence of one or two UAS transgenes as the
315 efficiency of *R86E01-GAL4* in driving the expression of either was comparable as
316 shown by the similar GFP levels (Figures 2A–C, I, and J).

317 In mammals, the hallmarks of astrocyte activation are hypertrophy of astrocytes
318 and upregulated level of the glial fibrillary acidic protein (GFAP) (Pekny et al., 2004).
319 Given that there's no GFAP homolog in *Drosophila (*Doherty et al., 2009), we
320 examined morphological changes in astrocytes at single-cell resolution following TBI
321 by mosaic analysis with a repressible cell marker (MARCM) on adult fly brains at
322 3–4 days after eclosion. The cell bodies of these astrocytes were located at the
323 interface between neuropil and cortex regions, or in neuropils, and their cellular
324 processes infiltrated into neuropils (Figure 2E). Interestingly, astrocytes in injured
325 brains exhibited bright and distinct GFP^+ accumulations associated with their cellular
326 processes at 24 h after TBI (Figures 2F and 2G). Quantitatively, the number of these
327 accumulations per square nanometer in the cellular processes was significantly
328 increased at 24 h after TBI; the increase in the number of accumulations might be
329 responsible for the increase in GFP intensity triggered by TBI (Figure 2G).
330 Importantly, the diameter of astrocytes cell bodies was also increased at 24 h after
331 injury (Figure 2H). Taken together, these results show that astrocytes become reactive

332 in adult brains at 24 h after TBI.

333 Axotomy induces expression of injury-related proteins such as extracellular
334 proteases the matrix metalloprotease (MMP) (Purice et al., 2017). In addition to the
335 morphological changes in astrocytes, we observed upregulated expression of Mmp1
336 in TBI-treated brains (Figures 2I–J'', 2M–N'', and 2Q). These Mmp1^{+} signals were
337 colocalized with membrane-bound *mCD8::GFP* driven by the astrocytes-specific
338 driver *R86E01-GAL4* or ENG-specific driver *R56F03-GAL4* (Figures 2K, 2L, 2O, and
339 2P), with a more dominant expression in ENG. These results suggest that Mmp1
340 might be produced from both types of glia after TBI.

341

342 **Transcriptional profiling of astrocytes in adult flies reveals elevated expression of**
343 **injury-related genes upon TBI**

344 To further investigate how astrocytes respond to TBI, we analyzed transcriptional
345 changes in astrocytes by RNA-seq (Figure 3A). Due to the tiny soma and
346 morphological complexity, the analysis of a purified population of glial cells has been
347 difficult and technically challenging. We have optimized a protocol for purifying
348 astrocytes from adult Drosophila of *R86E01-Gal4>UAS-Redstinger* by
349 fluorescence-activated cell sorting (FACS) (see details in Materials and Methods). As
350 FACS removes most cell masses and RFP-negative cells, the remaining RFP^{+} cells are
351 mostly viable, as shown by MitoTracker staining, and purity was 92.96% (RFP^{+} and
352 MitoTracker^{+} cells/total cells) in uninjured brains (Figures S1A-C'). Further analysis
353 of the RNA-seq data showed that the astrocyte markers *Eaat1* (110359 reads) and
354 *alrm* (186413 reads) were highly expressed, while *nSyb*, a neuronal marker, was
355 hardly detected (125 reads) at 4 h after TBI, verifying the purity of FACS-sorted
356 astrocytes. A principal component analysis (PCA) revealed that the variance between
357 different groups (no injury vs. 4 h and 24 h after injury) was greater than the variance
358 within groups (Figure S1D). From analysis on five biological replicates for each time
359 point (no injury, 4 h, and 24 h after injury), we obtained 539 million reads (an average

360 of 36 million reads per sample) and aligned the RNA-seq reads to the *Drosophila*
361 genome. We found that 93.67 ± 0.89% of reads mapped to the *Drosophila* genome
362 (dm6 version). Using a cutoff of ≥ 2-fold differential expression (adj. *p* value <0.01,
363 Benjamini-Hochberg procedure), we identified 522 and 357 genes with altered
364 expression at 4 h (416 upregulated and 106 downregulated) and 24 h (229 upregulated
365 and 128 downregulated) after injury, respectively (Figures 3B–D; Table S2).

366 Gene Ontology (GO) analysis of these upregulated genes revealed that a
367 significant proportion were associated with endosomal transport, actin cytoskeleton,
368 and wound healing (Figure S2). Furthermore, we detected upregulated expression of
369 components functioning in the innate immune response after TBI. For instance,
370 expression of the components Relish and Dif of the Toll and Imd pathways was
371 upregulated in astrocytes after TBI (Figure 3D), in agreement with a previous finding
372 that Relish is necessary for TBI-induced secondary injuries (Swanson et al., 2020). In
373 addition, expression of injury-related genes including *chic*, *Jra*, *kay, rl*, *Cad96Ca*,
374 *Idgf4*, *Stam*, *draper*, *Pvr*, *spict*, *Mmp1* and *NijA*, and receptor genes including *Pvr*,
375 *draper*, *AdoR*, *PGRP-SA*, and *NimA* were upregulated in astrocytes at 4 h or 24 h after
376 injury (Table S3). A set of endocytic trafficking genes was also identified, including
377 *Arpc1*, *Arpc2*, *cpa*, *cpb*, *Stam*, and *Chmp1*. Subsequent RT-qPCR experiments
378 confirmed the upregulation of all six genes tested at 4 h and/or 24 h after TBI (Figure
379 3E), supporting the robustness of the RNA-seq analysis. As a control, the
380 astrocytes-specific *alrm* gene showed no upregulation upon TBI by RT-qPCR and
381 RNA-seq. Taken together, these findings validate the approach of RNA-seq
382 transcription profiling in detecting genes functionally related to injury responses in
383 astrocytes following TBI.

384

385 **Pvr and AP-1 are required for the upregulation of Mmp1 after TBI**

386 Among the candidates exhibiting upregulated expression in astrocytes upon TBI,
387 three receptors (Pvr, AdoR and Draper), all acting upstream of and activating the JNK

388 pathway (Ishimaru et al., 2004; Macdonald et al., 2013; Poernbacher and Vincent,
389 2018), emerged as new factors with uncharacterized functions in astrocytes (Figure
390 3D). The *Drosophila* RNA interference (RNAi) Screening Center Integrative
391 Ortholog Prediction Tool (DIOPT) identified orthologs of these three receptors,
392 subunits of transcriptional factor AP-1 (composed of Jra and kay) of the JNK pathway,
393 Mmp1, and endocytic trafficking genes in mouse and human (Table 1) (Hu et al.,
394 2011). These proteins mediate essential injury responses in vertebrates (Borea et al.,
395 2016; Motz and Coukos, 2013; Shi et al., 2021). To examine a potential role of the
396 receptors and their downstream signaling components in astrocytes after TBI, we
397 quantified the immunostaining intensity of these proteins from projected images of
398 the whole brain (including 20-30 slices with 1 μm per slice). As our RNA-seq analysis
399 revealed elevated expression of JNK-related injury genes such as *AP-1* and *Mmp1*
400 (Figure 3D and Table 1), we analyzed the expression of Mmp1, a transcriptional target
401 of AP-1 (Purice et al., 2017), as a readout for the activity of JNK signaling in response
402 to TBI. We found that upregulated Mmp1 expression induced by TBI was potently
403 suppressed by knocking down the expression of Pvr, Jra or kay (Figures 4A−D, 4F),
404 indicating that Mmp1 upregulation is mediated by Pvr and AP-1, and predominantly
405 occurrs in astrocytes. We note that the location and intensity of Mmp1 signals are
406 variable among different individuals (Figure 4), probably because the brain damage
407 caused by HIT is not stereotypical.

408 Even though flies with Draper knockdown in astrocytes exhibited high mortality,
409 analysis of escapers indicated that Mmp1 upregulation upon TBI was not completely
410 inhibited by Draper knockdown (Figure 4E and 4F). Knockdown of the other receptor
411 AdoR in astrocytes caused a weak inhibition of AP-1 and Mmp1 upregulation (Figure
412 S3A–A", S4G–H", S4I and S4J); *TRE-dsRed* that expresses the red fluorescent protein
413 dsRed under the control of 4 × AP-1 motifs (Chatterjee and Bohmann, 2012) was used
414 as a reporter for AP-1 activity. As Pvr showed the strongest regulation on Mmp1
415 expression among the three receptors (Figure 4 and S3), we focused on the potential

416 role of Pvr in astrocytes following TBI in the present study. It is noteworthy to
417 mention that although Draper expression was upregulated upon axotomy (MacDonald
418 et al., 2006) and TBI (Figure 3D), inhibiting Draper expression in astrocytes did not
419 suppress the Mmp1 upregulation after TBI (Figure 4E and 4F). Taken together, these
420 results suggest that Pvr, but not Draper, and AP-1 are required for upregulated Mmp1
421 in astrocytes after TBI.
422
423 **Pvr positively regulates AP-1 signaling and Mmp1 expression in astrocytes after**
424 **TBI**
425 We next investigated the genetic pathway by which Pvr functions in astrocytes in
426 response to TBI. We examined the activity of AP-1 using the *in vivo* reporter
427 TRE-dsRed (Chatterjee and Bohmann, 2012). In uninjured brains, we detected low
428 TRE-dsRed levels, suggesting a basal AP-1 activity (Figure 5A–A"). Similar to Mmp1,
429 TRE-dsRed levels were robustly upregulated at 24 h after TBI, suggesting activation
430 of JNK/AP-1 signaling (Figure 5B–B"). Importantly, TBI-induced expression of
431 TRE-dsRed and Mmp1 was suppressed or further upregulated when inhibiting or
432 overexpressing Pvr expression in astrocytes, respectively (Figure 5C – F").
433 Overexpression of Jra or kay alone did not affect expression of TRE-dsRed or Mmp1
434 (Figure S3A–F", 5I and 5J), suggesting that overexpressing a single subunit of the
435 AP-1 complex is not sufficient to upregulate AP-1 activity. While Pvr overexpression
436 caused an increase in TRE-dsRed and Mmp1 expression levels, *Jra* or *kay* RNAi
437 knockdown in the background of Pvr overexpression suppressed the increase (Figure
438 5G–L), indicating that Jra and kay act downstream of Pvr to mediate the injury
439 response upon TBI. These results together show that Pvr is a receptor acting upstream
440 of AP-1 signaling that promotes Mmp1 expression during the injury response in
441 astrocytes (Figure 5M).
442

443 **Disruption of endocytosis and endocytic trafficking enhances Pvr, AP-1, and**
444 **Mmp1 upregulation upon TBI**

445 How was the Pvr signalling induced by TBI regulated? It has been shown that
446 VEGFR2 endocytosis proceeds in a clathrin-dependent manner (Simons et al., 2016).
447 During clathrin-dependent endocytosis, scission needs Cdc42-interacting protein 4
448 (Cip4) to recruit dynamin and Wiskott-Aldrich syndrome protein (WASp), the
449 activator of the Arp2/3 complex that mediates actin polymerization and promotes the
450 movement of newly-formed clathrin-coated vesicles (Brüser and Bogdan, 2017).
451 VEGFRs are transmembrane RTKs that are activated when they locate at the cell
452 membrane (Simons et al., 2016). We first investigated whether endocytosis is
453 involved in Pvr signaling upon TBI. *Shibire* (*shi*) encodes a GTPase called dynamin
454 which is responsible for fission of the vesicle from the membrane (van der Bliek and
455 Meyerowitz, 1991). We analysed the effect of endocytosis on Pvr signaling by
456 blocking the activity of dynamin with a temperature sensitive mutant, shi^{ts}, in
457 astrocytes. Interestingly, both Pvr (Figures 6A, 6B, and 6E) and TRE-dsRed (Figures
458 6C, 6D, and 6F) intensities were increased at 4 h after TBI when dynamin activity
459 was blocked at the non-permissive 32°C. As a control, expression of nLacZ under the
460 same conditions as mutated dynamin did not exhibit a significant difference in the
461 intensities of Pvr and TRE-dsRed at the permissive 23°C and the non-permissive
462 32°C after TBI (Figures 6A, 6B, 6E, and 6F). These results suggest that Pvr signaling
463 is facilitated when endocytosis is blocked.

464 In addition to Pvr, results from our transcription profiling analysis also revealed
465 upregulation of the expression of actin dynamics and endocytic trafficking genes
466 including *Arpc2*, *cpa*, and *cpb* following TBI (Tables 1 and S2). To explore whether
467 endocytic trafficking genes are involved in the injury response in astrocytes, we
468 analyzed Mmp1 and TRE-dsRed expression when inhibiting the expression of Arpc2,
469 cpa, or cpb. Interestingly, TBI-induced Mmp1 levels were further increased after
470 knockdown of each of the three (Figures 7A–D, 7O); consistently, TRE-dsRed

471 expression was also increased after knockdown of *cpa* or *cpb* (Figures 7H–K, 7P).
472 These results indicate that genes involved in endocytosis and endocytic trafficking
473 normally inhibit induction of AP-1 and Mmp1 by TBI in astrocytes.

474 In addition, we also observed upregulated expression of a set of endosomal
475 sorting genes, including *Stam*, *Chmp1*, and *Vps24* that encode components of the
476 endosomal sorting complex required for transport (ESCRT)in astrocytes in response
477 to TBI (Tables 1 and S2). These genes are implicated in the formation of intraluminal
478 vesicles (ILVs) from multivesicular bodies (MVBs). Inhibiting expression of the
479 ESCRT-0 subunit Stam and the ESCRT-III subunits Chmp1 or Vps24 in astrocytes
480 however did not result in a significant difference in Mmp1 or TRE-dsRed expression
481 levels compared with controls following TBI (Figure 7E–G, 7L-N, 7O and 7P),
482 suggesting that endosome sorting in MVB may not affect Pvr signaling activity.

483

484 **Discussion**

485 Using a previously established a *Drosophila* TBI model, we found that TBI
486 causes neuronal apoptosis, BBB/BEB disruption, and astrocyte swelling. Astrocytes
487 respond to TBI by elevated Pvr expression, which in turn enhances the expression of
488 the downstream effectors AP-1 and Mmp1. Our findings identify a new signaling
489 pathway upregulated in astrocytes following TBI.

490 Unlike vertebrates, in which astrocytes become reactive (reactive astrogliosis)
491 and actively clear neuronal and synaptic debris via phagocytosis upon axon injury
492 (Liddelow and Barres, 2017), axon transection in *Drosophila* shows no immediate
493 astrocytic response to injury (Doherty et al., 2009; Purice et al., 2017). Instead,
494 *Drosophila* ENG express key components of the phagocytic machinery and engulf
495 neuronal debris in response to axotomy (Doherty et al., 2009). Here, we examined for
496 the molecular and cellular changes of astrocytes after TBI. Upon TBI, astrocytes
497 exhibited apparent damage response including enlarged soma and altered cellular
498 processes containing more membrane-bound GFP^+ accumulations (Figure 2A – J).

499 These findings suggest that astrocytes are activated upon TBI, demonstrating a critical
500 role for astrocytes in the injury response.

501 The innate immune response in *Drosophila* relies on the activation of multiple
502 signaling pathways including NF-κB/Relish-mediated Imd and Doral/Dif-mediated
503 Toll signaling pathways. Interestingly, our RNA-seq data revealed elevated expression
504 of genes *Relish* and *Dif* in both pathways upon TBI (Figure 3D). However, the
505 expressions of *AMPs* were minimum in astrocytes before TBI and no AMPs genes
506 were identified in differentially expressed genes. Thus, AMPs genes were not
507 activated in astrocytes, though upregulated *AMP* expressions were detected by bulk
508 RNA-seq after TBI. In addition, expression of AP-1 (composed of Jra and kay) and
509 Mmp1 was also upregulated, indicating that the AP-1signaling pathway is activated in
510 astrocytes following TBI. Even though upregulated Mmp expression in reactive glial
511 responses is an evolutionarily conserved feature of *Drosophila* and mammalian glia
512 (Cunningham et al., 2005; Purice et al., 2017), transmembrane receptors on astrocytes
513 that regulate Mmp1 expression have not been identified. In mammals, knockdown of
514 VEGF signaling in keratinocytes reduced angiogenesis and delayed wound healing
515 (Rossiter et al., 2004). In *Drosophila,* studies of wound healing showed that Pvr likely
516 acts upstream of actin regulatory proteins that promote actin polymerization to lead
517 cells migration (Brock et al., 2012; Wu et al., 2009).

518 Through a combination of RNA-seq and genetic analyses, we identified Pvr as a
519 new receptor in astrocytes; Pvr promotes Mmp1 expression via the transcription
520 factor complex AP-1. At present, we do not know how Pvr promotes expression of
521 AP-1 and Mmp1. But previous findings show that Pvr phosphorylates JNK to trigger
522 the downstream signaling containing AP-1 during thorax closure in metamorphosis
523 (Ishimaru et al., 2004). During development, the midline glia survival and migration
524 are regulated by the ventral unpaired median (VUM) and the midline precursor 1
525 (MP1) midline neurons, the sources of Pvr ligands, i.e., PDGF- and VEGF-related
526 factor 1-3 (Pvf1-3) (Learte et al., 2008). Additionally, epidermal cell-derived Pvf1

527 may be sequestered in the blood and exposed upon injury to bind Pvr receptors on
528 wound-edge epidermal cells and initiate the extension of cell processes into the
529 wound gap (Wu et al., 2009). Specifically, Pvr ligands bind to Pvr receptor to induce
530 autophosphorylation of tyrosine residues, leading to JNK phosphorylation.
531 Phosphorylated JNK (Bsk) then phosphorylates Jun/Jra transcription factors,
532 triggering Jun/Jra association with Fos/kay, to form the AP-1 complex (Bogoyevitch
533 and Kobe, 2006). In addition, glial AP-1 is essential for recovery, ensuring brain
534 integrity and animal survival in the early post-TBI period (Byrns et al., 2021). Given
535 that Pvr and AP-1 genetically interact in astrocytes upon TBI, it is likely that Pvr acts
536 upstream of AP-1 and regulates its activity via JNK phosphorylation following brain
537 injury. We speculate that Pvr ligands that may secret from injured cells to activate
538 Pvr-positive astrocytes after TBI; activated Pvr then increases Mmp1 expression via
539 AP-1 and secretion to the intercellular space to participate in injury response.

540 In addition to Pvr, our RNA-seq data also identified other receptors potentially
541 functioning in astrocytes in response to TBI. Specifically, AdoR expression was
542 upregulated after TBI (Table S2), and knockdown of AdoR expression in astrocytes
543 led to inhibition of AP-1 after TBI (Figure S3G–J), though at a weaker extent
544 compared with Pvr knockdown. In mammals, $A_{2B}R$, a subtype of AdoR, was shown to
545 stimulate VEGF production in various cell types (Borea et al., 2016). Pvr promotes
546 the expression of adenosine deaminase-related growth factor A (Adgf-A) which
547 inactivates extracellular adenosine, the ligand of AdoR (Zurovec et al., 2002).
548 Furthermore, Pvr and AdoR collaborate in differentiating cells to maintain the
549 expression of Adgf-A (Mondal et al., 2011). Thus, it is possible that Pvr and AdoR act
550 independently or in a coordinated manner to regulate the injury response to TBI in
551 astrocytes in *Drosophila*.

552 Our RNA-seq profiling also revealed upregulation of Draper. Previous studies
553 revealed a role for Draper-mediated phagocytosis of axonal debris in ENG after
554 axotomy (Lu et al., 2017; MacDonald et al., 2006); axotomy induces Wallerian-like

555 degeneration (Büki and Povlishock, 2006; Tang-Schomer et al., 2010). Specifically,
556 damage-associated molecular pattern (DAMP) proteins released from injured neurons
557 bind to Draper and activate the JNK and JAK/STAT pathways in ENG (Doherty et al.,
558 2014; Freeman, 2015; MacDonald et al. 2013). Here, our findings showed that Draper
559 does not affect Mmp1 expression in astrocytes upon TBI. Although an increase in
560 Draper expression was detected in astrocytes by RNA-seq, knockdown of its
561 expression did not significantly suppress Mmp1 upregulation after TBI. Thus, Draper
562 activates JNK/AP-1 and JAK/STAT signaling in ENG in response to axotomy
563 (Doherty et al., 2014; MacDonald et al. 2013), whereas astrocytes respond to TBI via
564 Pvr-mediated AP-1 signaling. Despite different pathways are activated in different
565 types of glia upon brain injury, they may cooperate in response to TBI.

566 Endocytosis and trafficking of VEGFR, the mammalian Pvr homolog, regulate
567 the specificity as well as the duration and strength of the signaling output (Simons et
568 al., 2016). Once activated on the plasma membrane and translocated into the
569 cytoplasm, VEGFRs are either shuttled to lysosomes for degradation or recycled back
570 to the plasm membrane to replenish the receptor pool (Simons et al., 2016). Our
571 findings showed that disruption of endocytosis by disrupting dynamin activity and
572 inhibiting the expression of Arpc2, cpa, or cpb that regulate endocytic transport into
573 early endosomes enhanced the AP-1 and Mmp1 upregulation in astrocyte following
574 TBI (Figures 7A–D, 7H–K, 7O, 7P). As receptor endocytosis attenuates the strength
575 or duration of many signaling processes by physically reducing the concentration of
576 cell surface receptors accessible to the ligand (Jékely et al., 2005), blocking
577 dynamin-mediated endocytosis and endocytic trafficking potentially results in
578 accumulated Pvr receptors on the plasma membrane to activate the downstream
579 effector AP-1, thereby enhancing the astrocytes response to TBI. On the other hand,
580 ubiquitinated RTKs are recognized by ESCRT-0, followed by sequential recruitment
581 of ESCRT-I, ESCRT-II, and ESCRT-III onto the membranes of MVBs to form
582 intraluminal vesicles (ILVs) (Goh and Sorkin, 2013). Knockdown of the ESCRT-0

583 subunit Stam and the ESCRT-III subunits Chmp1 and Vps24 did not affect the
584 expression of Pvr downstream signaling components (Figure 7E–G, 7L–N, 7O and
585 7P), suggesting that Pvr signal transduction was not regulated by endosomal sorting.
586 Considering the importance of VEGF signaling in a variety of cellular processes,
587 including wound repair (Folkman and Klagsbrun, 1987), elucidating the downstream
588 signaling mechanisms, as well as defining the full array of Pvr targets in healthy and
589 diseased brains, will be critical for dissecting the protective or detrimental roles of
590 VEGF in the context of brain injury. Given that the Pvr receptor, AP-1, and the MMP
591 family of secreted proteases are all highly conserved across species, our work
592 provides new insights into how VEGF signaling in glia mechanistically contributes to
593 the TBI response in mammals.
594

595 **Acknowledgements**

596 This work was supported in part by the Ministry of Science and Technology of China
597 (2019YFA0707100 and 2021ZD0203900 to Y.Q. Zhang), the National Natural Science
598 Foundation of China (31921002, 31830036, and 31861143031 to Y.Q. Zhang,
599 32170962 to M. Ho and 31500839 to C.X. Mao), the Chinese Academy of Sciences
600 Strategic Priority Research Program B grants (XDBS1020100 to Y.Q. Zhang). We
601 thank Bloomington and Tsinghua stock centers for providing fly stocks. We are also
602 grateful to Zhiguo Ma, Oren Schuldiner, Sean Speese, Yong Zhang, Zhiyong Liu, and
603 the members of the Yong Q. Zhang lab for discussion and suggestions.
604

605 **References**

606 Apte, R. S., Chen, D. S., Ferrara, N. (2019). VEGF in Signaling and Disease: Beyond
607 Discovery and Development. *Cell*, *176*(6), 1248-1264.
608 Awasaki, T., Tatsumi, R., Takahashi, K., Arai, K., Nakanishi, Y., Ueda, R., Ito, K.
609 (2006). Essential role of the apoptotic cell engulfment genes draper and ced-6 in
610 programmed axon pruning during Drosophila metamorphosis. *Neuron*, *50*(6),

611 855-867.
612 Ayaz, D., Leyssen, M., Koch, M., Yan, J., Srahna, M., Sheeba, V., Hassan, B. A.
613 (2008). Axonal injury and regeneration in the adult brain of Drosophila. *Journal of*
614 *Neuroscience*, *28*(23), 6010-6021.
615 Bainton, R. J., Tsai, L. T., Schwabe, T., DeSalvo, M., Gaul, U., Heberlein, U. (2005).
616 moody encodes two GPCRs that regulate cocaine behaviors and blood-brain barrier
617 permeability in Drosophila. *Cell*, *123*(1), 145-156.
618 Barekat, A., Gonzalez, A., Mauntz, R. E., Kotzebue, R. W., Molina, B.,
619 El-Mecharrafie, N., Ratliff, E. P. (2016). Using Drosophila as an integrated model to
620 study mild repetitive traumatic brain injury. *Sci Rep*, *6*, 25252.
621 Bier, E. (2005). Drosophila, the golden bug, emerges as a tool for human genetics.
622 *Nature Reviews. Genetics*, *6*(1), 9-23.
623 Bogoyevitch, M. A., Kobe, B. (2006). Uses for JNK: the many and varied substrates
624 of the c-Jun N-terminal kinases. *Microbiology and Molecular Biology Reviews*, *70*(4),
625 1061-1095.
626 Bolger, A. M., Lohse, M., Usadel, B. (2014). Trimmomatic: a flexible trimmer for
627 Illumina sequence data. *Bioinformatics*, *30*(15), 2114-2120.
628 Borea, P. A., Gessi, S., Merighi, S., Varani, K. (2016). Adenosine as a Multi-Signaling
629 Guardian Angel in Human Diseases: When, Where and How Does it Exert its
630 Protective Effects? *Trends in Pharmacological Sciences*, *37*(6), 419-434.
631 Brock, A. R., Wang, Y., Berger, S., Renkawitz-Pohl, R., Han, V. C., Wu, Y., Galko, M.
632 J. (2012). Transcriptional regulation of Profilin during wound closure in Drosophila
633 larvae. *Journal of Cell Science*, *125*(Pt 23), 5667-5676.
634 Brüser, L., Bogdan, S. (2017). Adherens Junctions on the Move-Membrane
635 Trafficking of E-Cadherin. *Cold Spring Harbor Perspectives in Biology*, *9*(3).
636 Büki, A., Povlishock, J. T. (2006). All roads lead to disconnection?--Traumatic axonal
637 injury revisited. *Acta Neurochirurgica*, *148*(2), 181-193; discussion 193-184.
638 Burda, J. E., Sofroniew, M. V. (2014). Reactive gliosis and the multicellular response

639 to CNS damage and disease. *Neuron*, *81*(2), 229-248.
640 Byrns C. N., Saikumar J., Bonini N. M. (2021). Glial AP1 is activated with aging and
641 accelerated by traumatic brain injury. *Nat. Aging*, *1*(7), 585-597.
642 Chatterjee, N., Bohmann, D. (2012). A versatile ΦC31 based reporter system for
643 measuring AP-1 and Nrf2 signaling in Drosophila and in tissue culture. *PLoS ONE*,
644 *7*(4), e34063.
645 Cho, N. K., Keyes, L., Johnson, E., Heller, J., Ryner, L., Karim, F., Krasnow, M. A.
646 (2002). Developmental control of blood cell migration by the Drosophila VEGF
647 pathway. *Cell*, *108*(6), 865-876.
648 Chodobski, A., Zink, B. J., Szmydynger-Chodobska, J. (2011). Blood-brain barrier
649 pathophysiology in traumatic brain injury. *Transl Stroke Res*, *2*(4), 492-516.
650 Cunningham, L. A., Wetzel, M., Rosenberg, G. A. (2005). Multiple roles for MMPs
651 and TIMPs in cerebral ischemia. *Glia*, *50*(4), 329-339.
652 Daneshvar, D. H., Goldstein, L. E., Kiernan, P. T., Stein, T. D., McKee, A. C. (2015).
653 Post-traumatic neurodegeneration and chronic traumatic encephalopathy. *Molecular*
654 *and Cellular Neurosciences*, *66*(Pt B), 81-90.
655 Davalos, D., Grutzendler, J., Yang, G., Kim, J. V., Zuo, Y., Jung, S., Gan, W. B. (2005).
656 ATP mediates rapid microglial response to local brain injury in vivo. *Nature*
657 *Neuroscience*, *8*(6), 752-758.
658 Doherty, J., Logan, M. A., Tasdemir, O. E., Freeman, M. R. (2009). Ensheathing glia
659 function as phagocytes in the adult Drosophila brain. *Journal of Neuroscience*, *29*(15),
660 4768-4781.
661 Doherty, J., Sheehan, A. E., Bradshaw, R., Fox, A. N., Lu, T. Y., Freeman, M. R.
662 (2014). PI3K signaling and Stat92E converge to modulate glial responsiveness to
663 axonal injury. *PLoS Biology*, *12*(11), e1001985.
664 Egeblad, M., Werb, Z. (2002). New functions for the matrix metalloproteinases in
665 cancer progression. *Nature Reviews. Cancer*, *2*(3), 161-174.
666 Folkman, J., Klagsbrun, M. (1987). Angiogenic factors. *Science*, *235*(4787), 442-447.

667 Freeman, M. R. (2015). Drosophila Central Nervous System Glia. *Cold Spring*
668 *Harbor Perspectives in Biology*, *7*(11).
669 Goh, L. K., Sorkin, A. (2013). Endocytosis of receptor tyrosine kinases. *Cold Spring*
670 *Harbor Perspectives in Biology*, *5*(5), a017459.
671 Hoch, R. V., Soriano, P. (2003). Roles of PDGF in animal development. *Development*,
672 *130*(20), 4769-4784.
673 Hoopfer, E. D., McLaughlin, T., Watts, R. J., Schuldiner, O., O'Leary, D. D., Luo, L.
674 (2006). Wlds protection distinguishes axon degeneration following injury from
675 naturally occurring developmental pruning. *Neuron*, *50*(6), 883-895.
676 Hu, Y., Flockhart, I., Vinayagam, A., Bergwitz, C., Berger, B., Perrimon, N., Mohr, S.
677 E. (2011). An integrative approach to ortholog prediction for disease-focused and
678 other functional studies. *BMC Bioinformatics*, *12*, 357.
679 Ishimaru, S., Ueda, R., Hinohara, Y., Ohtani, M., Hanafusa, H. (2004). PVR plays a
680 critical role via JNK activation in thorax closure during Drosophila metamorphosis.
681 *EMBO Journal*, *23*(20), 3984-3994.
682 Jékely, G., Sung, H. H., Luque, C. M., Rørth, P. (2005). Regulators of endocytosis
683 maintain localized receptor tyrosine kinase signaling in guided migration.
684 *Developmental Cell*, *9*(2), 197-207.
685 Jia, M., Meng, D., Chen, M., Li, T., Zhang, Y. Q., Yao, A. (2019). Drosophila
686 homolog of the intellectual disability-related long-chain acyl-CoA synthetase 4 is
687 required for neuroblast proliferation. *J Genet Genomics*, *46*(1), 5-17.
688 Joy, M. T., Ben Assayag, E., Shabashov-Stone, D., Liraz-Zaltsman, S., Mazzitelli, J.,
689 Arenas, M., Carmichael, S. T. (2019). CCR5 Is a Therapeutic Target for Recovery
690 after Stroke and Traumatic Brain Injury. *Cell*, *176*(5), 1143-1157.e1113.
691 Katzenberger, R. J., Chtarbanova, S., Rimkus, S. A., Fischer, J. A., Kaur, G., Seppala,
692 J. M., Wassarman, D. A. (2015). Death following traumatic brain injury in Drosophila
693 is associated with intestinal barrier dysfunction. *Elife*, *4*.
694 Katzenberger, R. J., Ganetzky, B., Wassarman, D. A. (2016). Age and diet affect

695 genetically separable secondary injuries that cause acute mortality following
696 traumatic brain injury in Drosophila. *G3 (Bethesda)*, *6*(12), 4151-66.
697 Katzenberger, R. J., Loewen, C. A., Wassarman, D. R., Petersen, A. J., Ganetzky, B.,
698 Wassarman, D. A. (2013). A Drosophila model of closed head traumatic brain injury.
699 *Proceedings of the National Academy of Sciences of the United States of America*,
700 *110*(44), E4152-4159. Kim, D., Langmead, B., Salzberg, S. L. (2015). HISAT: a fast
701 spliced aligner with low memory requirements. *Nature Methods*, *12*(4), 357-360.
702 Kim, D., Paggi, J. M., Park, C., Bennett, C., Salzberg, S. L. (2019). Graph-based
703 genome alignment and genotyping with HISAT2 and HISAT-genotype. *Nature*
704 *Biotechnology*, *37*(8), 907-915.
705 Kremer, M. C., Jung, C., Batelli, S., Rubin, G. M., Gaul, U. (2017). The glia of the
706 adult Drosophila nervous system. *Glia*, *65*(4), 606-638.
707 Learte, A. R., Forero, M. G., Hidalgo, A. (2008). Gliatrophic and gliatropic roles of
708 PVF/PVR signaling during axon guidance. *Glia*, *56*(2), 164-176.
709 Lee, T., Luo, L. (1999). Mosaic analysis with a repressible cell marker for studies of
710 gene function in neuronal morphogenesis. *Neuron*, *22*(3), 451-461.
711 Liddelow, S. A., Barres, B. A. (2017). Reactive Astrocytes: Production, Function, and
712 Therapeutic Potential. *Immunity*, *46*(6), 957-967.
713 Liddelow, S. A., Guttenplan, K. A., Clarke, L. E., Bennett, F. C., Bohlen, C. J.,
714 Schirmer, L., Barres, B. A. (2017). Neurotoxic reactive astrocytes are induced by
715 activated microglia. *Nature*, *541*(7638), 481-487.
716 Love, M. I., Huber, W., Anders, S. (2014). Moderated estimation of fold change and
717 dispersion for RNA-seq data with DESeq2. *Genome Biology*, *15*(12), 550.
718 Lu, T. Y., Doherty, J., Freeman, M. R. (2014). DRK/DOS/SOS converge with
719 Crk/Mbc/dCed-12 to activate Rac1 during glial engulfment of axonal debris. *Proc.*
720 *Natl. Acad. Sci. USA*, *111*(34), 12544-12549.
721 Lu, T. Y., MacDonald, J. M., Neukomm, L. J., Sheehan, A. E., Bradshaw, R., Logan,
722 M. A., Freeman, M. R. (2017). Axon degeneration induces glial responses through

723 Draper-TRAF4-JNK signaling. *Nature Communications*, *8*, 14355.
724 Ma, V. Y., Chan, L., Carruthers, K. J. (2014). Incidence, prevalence, costs, and impact
725 on disability of common conditions requiring rehabilitation in the United States:
726 stroke, spinal cord injury, traumatic brain injury, multiple sclerosis, osteoarthritis,
727 rheumatoid arthritis, limb loss, and back pain. *Archives of Physical Medicine and*
728 *Rehabilitation*, *95*(5), 986-995.e981.
729 MacDonald, J. M., Beach, M. G., Porpiglia, E., Sheehan, A. E., Watts, R. J., Freeman,
730 M. R. (2006). The Drosophila cell corpse engulfment receptor Draper mediates glial
731 clearance of severed axons. *Neuron*, *50*(6), 869-881.
732 Macdonald, J. M., Doherty, J., Hackett, R., Freeman, M. R. (2013). The c-Jun kinase
733 signaling cascade promotes glial engulfment activity through activation of draper and
734 phagocytic function. *Cell Death and Differentiation*, *20*(9), 1140-1148.
735 McDonald, J. A., Pinheiro, E. M., Montell, D. J. (2003). PVF1, a PDGF/VEGF
736 homolog, is sufficient to guide border cells and interacts genetically with Taiman.
737 *Development*, *130*(15), 3469-3478.
738 Mira, R. G., Lira, M., Cerpa, W. (2021). Traumatic Brain Injury: Mechanisms of Glial
739 Response. *Front Physiol*, *12*, 740939.
740 Mondal, B. C., Mukherjee, T., Mandal, L., Evans, C. J., Sinenko, S. A.,
741 Martinez-Agosto, J. A., Banerjee, U. (2011). Interaction between differentiating cell-
742 and niche-derived signals in hematopoietic progenitor maintenance. *Cell*, *147*(7),
743 1589-1600.
744 Moreno, E., Yan, M., Basler, K. (2002). Evolution of TNF signaling mechanisms:
745 JNK-dependent apoptosis triggered by Eiger, the Drosophila homolog of the TNF
746 superfamily. *Current Biology*, *12*(14), 1263-1268.
747 Motz, G. T., Coukos, G. (2013). Deciphering and reversing tumor immune
748 suppression. *Immunity*, *39*(1), 61-73. https://doi.org/10.1016/j.immuni.2013.07.005
749 Ng, S. Y., & Lee, A. Y. W. (2019). Traumatic Brain Injuries: Pathophysiology and
750 Potential Therapeutic Targets. *Front Cell Neurosci*, *13*, 528.

751 Page-McCaw, A., Ewald, A. J., Werb, Z. (2007). Matrix metalloproteinases and the
752 regulation of tissue remodelling. *Nature Reviews. Molecular Cell Biology*, *8*(3),
753 221-233.
754 Parks, W. C., Wilson, C. L., López-Boado, Y. S. (2004). Matrix metalloproteinases as
755 modulators of inflammation and innate immunity. *Nature Reviews. Immunology*, *4*(8),
756 617-629.
757 Pastor-Pareja, J. C., Grawe, F., Martín-Blanco, E., García-Bellido, A. (2004). Invasive
758 cell behavior during Drosophila imaginal disc eversion is mediated by the JNK
759 signaling cascade. *Developmental Cell*, *7*(3), 387-399.
760 Pekny M, Pekna M. (2004). Astrocyte intermediate filaments in CNS pathologies and
761 regeneration. *The Journal of Pathology, 204*(4):428-37.
762 Pertea, M., Kim, D., Pertea, G. M., Leek, J. T., Salzberg, S. L. (2016). Transcript-level
763 expression analysis of RNA-seq experiments with HISAT, StringTie and Ballgown.
764 *Nature Protocols*, *11*(9), 1650-1667.
765 Pfeiffer, B. D., Truman, J. W., Rubin, G. M. (2012). Using translational enhancers to
766 increase transgene expression in Drosophila. *Proceedings of the National Academy of*
767 *Sciences of the United States of America, 109*(17), 6626-6631.
768 Poernbacher, I., Vincent, J. P. (2018). Epithelial cells release adenosine to promote
769 local TNF production in response to polarity disruption. *Nature Communications*, *9*(1),
770 4675.
771 Purice, M. D., Ray, A., Munzel, E. J., Pope, B. J., Park, D. J., Speese, S. D., Logan, M.
772 A. (2017). A novel Drosophila injury model reveals severed axons are cleared through
773 a Draper/MMP-1 signaling cascade. *Elife*, *6*.
774 Rodríguez-Baeza, A., Reina-de la Torre, F., Poca, A., Martí, M., Garnacho, A. (2003).
775 Morphological features in human cortical brain microvessels after head injury: a
776 three-dimensional and immunocytochemical study. *Anatomical Record. Part A,*
777 *Discoveries in Molecular, Cellular, and Evolutionary Biology*, *273*(1), 583-593.
778 Rossiter, H., Barresi, C., Pammer, J., Rendl, M., Haigh, J., Wagner, E. F., Tschachler,

E. (2004). Loss of vascular endothelial growth factor a activity in murine epidermal keratinocytes delays wound healing and inhibits tumor formation. *Cancer Research*, *64*(10), 3508-3516.

Saikumar J, Byrns C. N., Hemphill M., Meaney D. F., Bonini N. M. (2020). Dynamic neural and glial responses of a head-specific model for traumatic brain injury in Drosophila. *Proceedings of the National Academy of Sciences of the United States of America*, 117(29):17269-77.

Sakurai, Y., Ohgimoto, K., Kataoka, Y., Yoshida, N., Shibuya, M. (2005). Essential role of Flk-1 (VEGF receptor 2) tyrosine residue 1173 in vasculogenesis in mice. *Proceedings of the National Academy of Sciences of the United States of America*, *102*(4), 1076-1081.

Sangiorgi, S., De Benedictis, A., Protasoni, M., Manelli, A., Reguzzoni, M., Cividini, A., Balbi, S. (2013). Early-stage microvascular alterations of a new model of controlled cortical traumatic brain injury: 3D morphological analysis using scanning electron microscopy and corrosion casting. *Journal of Neurosurgery*, *118*(4), 763-774.

Shi, X., Luo, L., Wang, J., Shen, H., Li, Y., Mamtilahun, M., Yang, G. Y. (2021). Stroke subtype-dependent synapse elimination by reactive gliosis in mice. *Nature Communications*, *12*(1), 6943.

Sil, S., Periyasamy, P., Thangaraj, A., Chivero, E. T., Buch, S. (2018). PDGF/PDGFR axis in the neural systems. *Molecular Aspects of Medicine*, *62*, 63-74.

Simons, M., Gordon, E., Claesson-Welsh, L. (2016). Mechanisms and regulation of endothelial VEGF receptor signaling. *Nature Reviews. Molecular Cell Biology*, *17*(10), 611-625.

Sofroniew, M. V., Vinters, H. V. (2010). Astrocytes: biology and pathology. *Acta Neuropathologica*, *119*(1), 7-35.

Stork, T., Sheehan, A., Tasdemir-Yilmaz, O. E., Freeman, M. R. (2014). Neuron-glia interactions through the Heartless FGF receptor signaling pathway mediate morphogenesis of Drosophila astrocytes. *Neuron*, *83*(2), 388-403.

807 Swanson, L. C., Trujillo, E. A., Thiede, G. H., Katzenberger, R. J., Shishkova, E.,
808 Coon, J. J., Ganetzky, B., Wassarman, D. A. (2020). Survival following traumatic
809 brain injury in Drosophila is increased by heterozygosity for a mutation of the
810 NF-kappaB innate immune response transcription factor Relish. *Genetics*, *216*(4),
811 1117-1136.
812 Tang-Schomer, M. D., Patel, A. R., Baas, P. W., Smith, D. H. (2010). Mechanical
813 breaking of microtubules in axons during dynamic stretch injury underlies delayed
814 elasticity, microtubule disassembly, and axon degeneration. *FASEB Journal*, *24*(5),
815 1401-1410.
816 Thacker, S. A., Bonnette, P. C., Duronio, R. J. (2003). The contribution of
817 E2F-regulated transcription to Drosophila PCNA gene function. *Current Biology*,
818 *13*(1), 53-58.
819 Valanne, S., Wang, J. H., Rämet, M. (2011). The Drosophila Toll signaling pathway.
820 *Journal of Immunology*, *186*(2), 649-656.
821 Van Alphen B., Stewart S., Iwanaszko M., Xu F, Li K., Rozenfeld S., Ramakrishnan
822 A., Itoh T. Q., Sisobhan S., Qin Z. et al., (2022). Glial immune-related pathways
823 mediate effects of closed head traumatic brain injury on behavior and lethality in
824 Drosophila. *PLoS Biololy*, *20*(1), e3001456.
825 Willsey, H. R., Zheng, X., Carlos Pastor-Pareja, J., Willsey, A. J., Beachy, P. A., Xu, T.
826 (2016). Localized JNK signaling regulates organ size during development. *Elife*, *5*.
827 A. M. van der Bliek, E. M. Meyerowitz (1991). Dynamin-like protein encoded by the
828 Drosophila shibire gene associated with vesicular traffic. *Nature, 351*(6325), 411-414.
829 Wu, Y., Brock, A. R., Wang, Y., Fujitani, K., Ueda, R., Galko, M. J. (2009). A
830 blood-borne PDGF/VEGF-like ligand initiates wound-induced epidermal cell
831 migration in Drosophila larvae. *Current Biology*, *19*(17), 1473-1477.
832 Yang, C. P., Fu, C. C., Sugino, K., Liu, Z., Ren, Q., Liu, L. Y., Lee, T. (2016).
833 Transcriptomes of lineage-specific Drosophila neuroblasts profiled by genetic
834 targeting and robotic sorting. *Development*, *143*(3), 411-421.

Yu, S., He, J. (2019). Stochastic cell-cycle entry and cell-state-dependent fate outputs of injury-reactivated tectal radial glia in zebrafish. *Elife*, *8*.

Zhao, K., Hong, H., Zhao, L., Huang, S., Gao, Y., Metwally, E., Zhang, Y. Q. (2020). Postsynaptic cAMP signaling regulates the antagonistic balance of Drosophila glutamate receptor subtypes. *Development*, *147*(24).

Zurovec, M., Dolezal, T., Gazi, M., Pavlova, E., Bryant, P. J. (2002). Adenosine deaminase-related growth factors stimulate cell proliferation in Drosophila by depleting extracellular adenosine. *Proceedings of the National Academy of Sciences of the United States of America*, *99*(7), 4403-4408.

845 ## Figure legends

846 **Figure 1. TBI is induced in adult flies by a high impact trauma (HIT) device.**
847 (A) MI_{24} is the mortality index calculated from the percentage of dead over total flies.
848 Increasing the number of strikes from 4 to 6 increases the MI_{24} value. Error bars
849 denote standard error of the mean (SEM; ***p <0.001, Student's t-test). (B–E) The
850 intactness of blood-eye-barrier (BEB) and blood-brain-barrier (BBB) before or after 6
851 strikes is indicated by the accumulated fluorescence intensity at the border of the eye
852 (B, D) and brain (C, E), respectively. The examination was carried out at 2 h after
853 fluorescent dye injection. Arrows indicate the hemolymph exclusion line. Scale bar =
854 100 μm. (F) The percentage of permeable BEB with or without TBI (***p <0.001).
855 (G) The percentage of permeable BBB following different numbers of strikes. Error
856 bars denote SEM (**p <0.01 and ***p <0.001, Student's t-test). (H) Histogram
857 showing mRNA expression levels of innate immune response genes of the AMP
858 family (*Attc*, *DiptB* and *Mtk*) in the adult brain. Expression was increased in all cases
859 following treatment. The *RPL28* gene served as an internal reference. Results are
860 means ± SEM (***p <0.001, Student's t-test). (I, J) The number of Dcp-1^+ puncta
861 (green) increased in injured adult brains 24 h after TBI. Scale bar = 50 μm. (K)
862 Quantification of Dcp-1^+ puncta. Error bars denote SEM (**p <0.01, Student's t-tests).
863 Results are means ± SEM. (L–M") Apoptotic debris labelled with anti-Dcp-1
864 antibodies (Red). Glial and neuronal nuclei are labelled with anti-Repo (L) and
865 anti-Elav (M) antibodies (Blue), respectively. Scale bar = 20 μm.

866

867 **Figure 2. TBI alters glial morphology and upregulates Mmp1 expression.**
868 (A–C) Representative images of astrocyte membranes labelled with *mCD8::GFP*
869 driven by the astrocyte driver *R86E01-Gal4*. Co-expression of *UAS-Redstinger* labels
870 astrocyte nuclei. GFP intensities are increased at 4 h (B) and 24 h (C) after injury. The
871 rectangle defined by white dash lines denotes antennal lobes. Scale bars = 100 μm. (D)
872 Quantification of GFP intensity at different timepoints after TBI. Results are

means ± SEM (**p <0.01, Student's t-test). (E, F) MARCM (*y w UAS-CD8::GFP hs-FLP; tubP-Gal80 FRT-40A/CyO; alrm-Gal4 UAS-CD8::GFP UAS-Dcr2/TM6 Tb Hu* cross with *FRT-40A* flies*)* analysis reveals single astrocytes with evenly distributed GFP^+ cellular processes without injury (E) and an increased number of GFP^+ puncta at 24 h after injury (F). Arrows denote GFP^+ accumulations in astrocyte processes. White dots demarcate neuropils. Anti-Repo antibodies labelled glial nuclei. TO-PRO labelled all nuclei. Insets show the morphology of a glial soma before and after injury. Scale bar = 10 μm. (G) Quantification of GFP^+ puncta in astrocyte processes before and after injury. (H) Quantification of the astrocyte soma diameter surrounding ALs after injury. Results are means ± SEM (***p <0.001, Student's t-test). (I–J", M–N") Representative images of ALs co-labelled with GFP and Mmp1 (magenta) in uninjured and injured adult brains. (J–J") GFP-labelled astrocyte membranes (green) overlapped with Mmp1 (magenta) after injury. (N–N") After injury, Mmp1 co-localizes with GFP-labelled ENG (*R56F03-Gal4*) membranes (green). Arrows show Mmp1-GFP colocalization in L" and P". Scale bar = 20 μm. (K, L) Graph showing fluorescence intensity per pixel in each channel for the inset in I" and J" of the astrocyte membrane and Mmp1 along a line drawn through a cell body. (O, P) Graph showing fluorescence intensity per pixel in each channel for the inset in M" and N" of the ENG membrane and Mmp1 along a line drawn through the process of ENG. (Q) Quantification of Mmp1 intensity in I–J" and M–N". Ast is the short of astrocytes. Results are means ± SEM (**p <0.01, Student's t-test).

Figure 3. Transcriptome analysis of astrocytes reveals upregulation of injury-related and innate immunity genes.

(A) After dissection, *Drosophila* brains were disrupted and the cell suspension was subjected to FACS. Astrocyte cDNAs were amplified by the Smart-seq2 method and a cDNA library was constructed. A subset of upregulated genes from RNA-seq screening was validated by quantitative real-time PCR. (B, C) Volcano plots of the

901 gene expression analysis; 522 differentially expressed genes (416 upregulated, 106
902 downregulated) in astrocytes were detected at 4 h after injury (B), and 357
903 differentially expressed genes (229 upregulated, 129 downregulated) in astrocytes
904 were detected at 24 h after injury (C). The threshold for differential expression was set
905 at $\log_2$FC = 1 with an adj. p <0.01. FC = fold change; adj. = adjusted (for multiple
906 comparisons by the Benjamin-Hochberg procedure). (D) Heatmap of the expression
907 of a small set of representative genes, including *draper*, *Jra* and *kay*, previously
908 identified as essential factors during glial clearance of severed axons. (E) Quantitative
909 real-time PCR validation of a subset of upregulated genes from RNA-seq screening.
910 Error bars represent SEM. Results are means ± SEM (*p <0.05, **p <0.01 and
911 ***p <0.001 by Student's t tests).
912
913 **Table 1. Upregulated genes related to receptors and endocytosis.**
914
915 **Figure 4. Pvr, Jra and kay are required for Mmp1 upregulation after TBI.**
916 (A–F) Knockdown of Pvr, Jra or kay by *R86E01-Gal4* driven RNAi in astrocytes
917 suppresses Mmp1 upregulation after TBI. Scale bar = 100 μm. All images are
918 projections of 25–30 μm immunostaining slices (one image per 1 μm slice). Arrows
919 show Mmp1 signals. (F) Quantification of Mmp1 intensity in different genotypes.
920 Results are means ± SEM (*p <0.05 by Student's t-test).
921
922 **Figure 5. Pvr is required for AP-1 upregulation after TBI.**
923 (A – B") Adult brains showing increased *TRE-dsRed* (an AP-1 reporter) expression at
924 24 h after TBI. (C – D") Overexpression of Pvr in astrocytes leads to upregulated
925 dsREd expression compared with control flies. Scale bar = 100 μm. (E – F")
926 Knockdown of Pvr in astrocytes causes downregulation of dsRed expression
927 compared with control flies after TBI. (G–H") Overexpression of Pvr and knockdown
928 of Jra at the same time in astrocytes causes downregulation of dsRed and Mmp1 after

929 TBI compared with controls. (I−J") Overexpression of Pvr and knockdown of kay in
930 astrocytes at the same time causes downregulation of dsRed and Mmp1 after TBI
931 compared with controls. (K, L) Quantification of Mmp1 (K) and dsRed (L) intensity.
932 Results are means ± SEM ***p* <0.01, ****p* <0.001, Student's *t*-tests.
933
934 **Figure 6. Inhibition of dynamin activity increases the expression levels of Pvr**
935 **and dsRed after TBI.**
936 (A, B) Representative Pvr immunostaining (green), dsRed (magenta) and β-gal
937 intensity (gray) in control animals (*TRE-dsRed;R86E01-Gal4>UAS-nLacZ*) at 4 h
938 after TBI. All images are projections of 25–30 μm immunostaining slices (one image
939 per 1 μm slice). (C, D) Representative Pvr immunostaining (green), dsRed (magenta)
940 and Mmp1 intensity (gray) in shi^{ts}-expressing animals
941 (*TRE-dsRed;R86E01-Gal4>UAS-*shi^{ts}) at 4 h after TBI. For thermogenetic
942 inactivation of dynamin, flies after TBI were incubated at intermittent temperature at
943 32°C (32°C for 30 min, and then back to 23°C for 30 min, for four rounds, four hours
944 in total) until dissection. (E, F) Quantification of Pvr and dsRed intensity in different
945 genotypes. Results are means ± SEM (**p* <0.05).
946
947 **Figure 7. Knockdown of endocytic trafficking-related genes up-regulates**
948 **expression of AP-1 and Mmp1upon TBI**
949 (A, H) Representative Mmp1 immunostaining (magenta) and dsRed intensity
950 (magenta) in control animals (*R86E01-Gal4*) at 24 h after TBI. (B–D, I–K)
951 Knockdown of *Arpc2*, *cpa*, and *cpb* in astrocytes results in further upregulation of
952 Mmp1 and dsRed upon TBI. All images are projections of 25–30 μm immunostaining
953 slices (one image per 1 μm slice). (E–G, L–N) Knockdown of *Stam*, *Chmp1* or *Vps24*,
954 components of ESCRT, in astrocytes had no influence on Mmp1 and dsRed
955 upregulation compared with control after TBI (A, H). All images are projections of
956 25–30 μm immunostaining slices (one image per 1 μm slice). (O, P) Quantification of

Mmp1 and dsRed intensity in different genotypes. Results are means ± SEM (*p <0.05, **p <0.01, ***p <0.001, Student's t-tests). (Q) Schematic diagram of Pvr–AP-1–MMP1 signaling activated by TBI in astrocytes. AP-1 transcription factor complex is composed of Jra and kay.

962

963 **Figure S1. Sorting of adult astrocytes by FACS.**

964 (A) To discriminate between healthy and damaged or dying cells, side scatter (SSC-A,
965 log) and forward scatter (FSC-A, log) were plotted. Higher SSC-A signals indicate
966 increased granularity and therefore likely dying cells. Thus, one should define the
967 sorting gate as the population with the lower SSC-A signal (P1). (P2) Exclude cell
968 clusters by sorting only events with a low FSC width (FSC-W) versus similar area
969 (FSC-A) signal to get exact single cell. (P3) To gate for RFP^+ cells, plotted the signal
970 from the excitation of cells with the 568-nm laser (PE-Texas Red-A, log) against the
971 signal from the SSC-A. The population with the higher PE-Texas Red-A signal was
972 the candidate cells cluster. The strategy for FACS is shown at the lower right corner.
973 (B–C') A population of cells with strong RFP signal was purified from adult flies of
974 *R86E01-Gal4>UAS-Redstinger*. (B and B') Confocal images of representative
975 astrocytes before and after sorting by FACS. Scale bar = 50 μm. (C and C') As
976 cell-permeant MitoTracker labels mitochondria of live cells, cells after FACS both
977 labelled by RFP and MitoTracker. Scale bar = 10 μm. (D) A Principal Component
978 Analysis of all biological replicates (uninjured versus injured) revealing genes
979 expressed at absolute value of logarithmic fold change ($\log_2$FC) > 1.0.

980

981 **Figure S2. GO analysis of differentially expressed genes at 4 h and 24 h after**
982 **injury.**

983 Scatterplot showing GO functional enrichment results for differentially expressed
984 genes of astrocytes in the brain at 4 h (A) and 24 h (B) after injury, p <0.01.

985

986 **Figure S3. Overexpression of Jra or kay does not enhance the expression of**
987 **TRE-RFP and Mmp1 in adult brain after TBI.**

988 (A, B") Fly brains showing TRE-RFP expression before and 24 h after TBI. (C–F")
989 overexpression of Jra or kay in astrocytes shows no apparent changes of RFP and

Mmp1 staining signals compared with control flies with or without brain injury (*TRE-dsRed/UAS-Jra* or *kay*; *R86E01-Gal4/+*). Scale bar = 100 μm. (G, H) Knockdown of AdoR in astrocytes inhibits the expression of Mmp1 after TBI. However, Knockdown of AdoR in astrocytes does not inhibit the expression of dsRed. (I, J) Quantification of Mmp1 and dsRed intensity before and after injury in different genotypes. Data are present as means ± SEM; $*p < 0.05$, $**p < 0.01$, $***p < 0.001$ by Student's *t* tests.

Figure 1

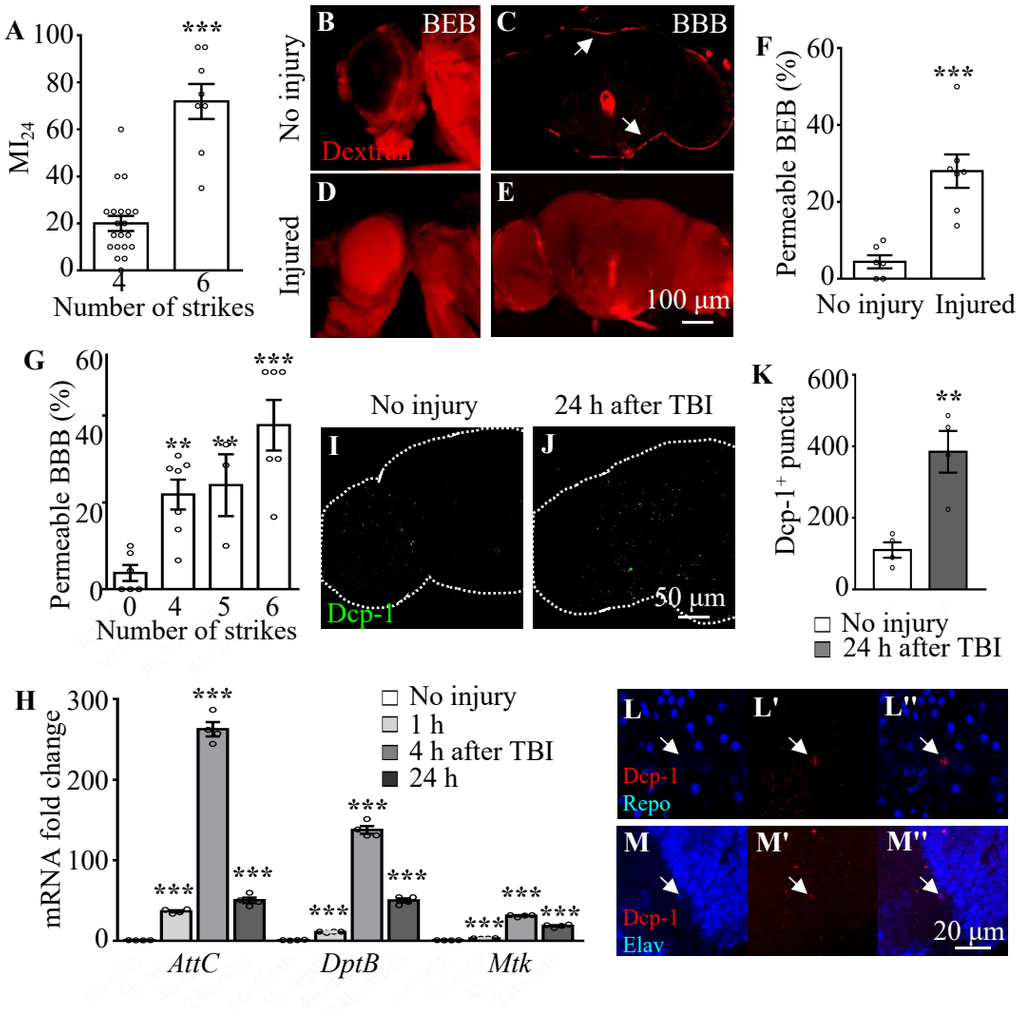
A
ML_{24}
Number of strikes
B BEB
C BBB
No injury
Injured
Dextran
D
E
100 µm
F
Permeable BEB (%)
No injury
Injured
G
Permeable BBB (%)
Number of strikes
No injury
24 h after TBI
I
J
Dcp-1
50 µm
K
Dcp-1+ puncta
No injury
24 h after TBI
H
mRNA fold change
No injury
1 h
4 h after TBI
24 h
AttC
DptB
Mtk
L
L'
L''
Dcp-1
Repo
M
M'
M''
Dcp-1
Elav
20 µm

Figure 2

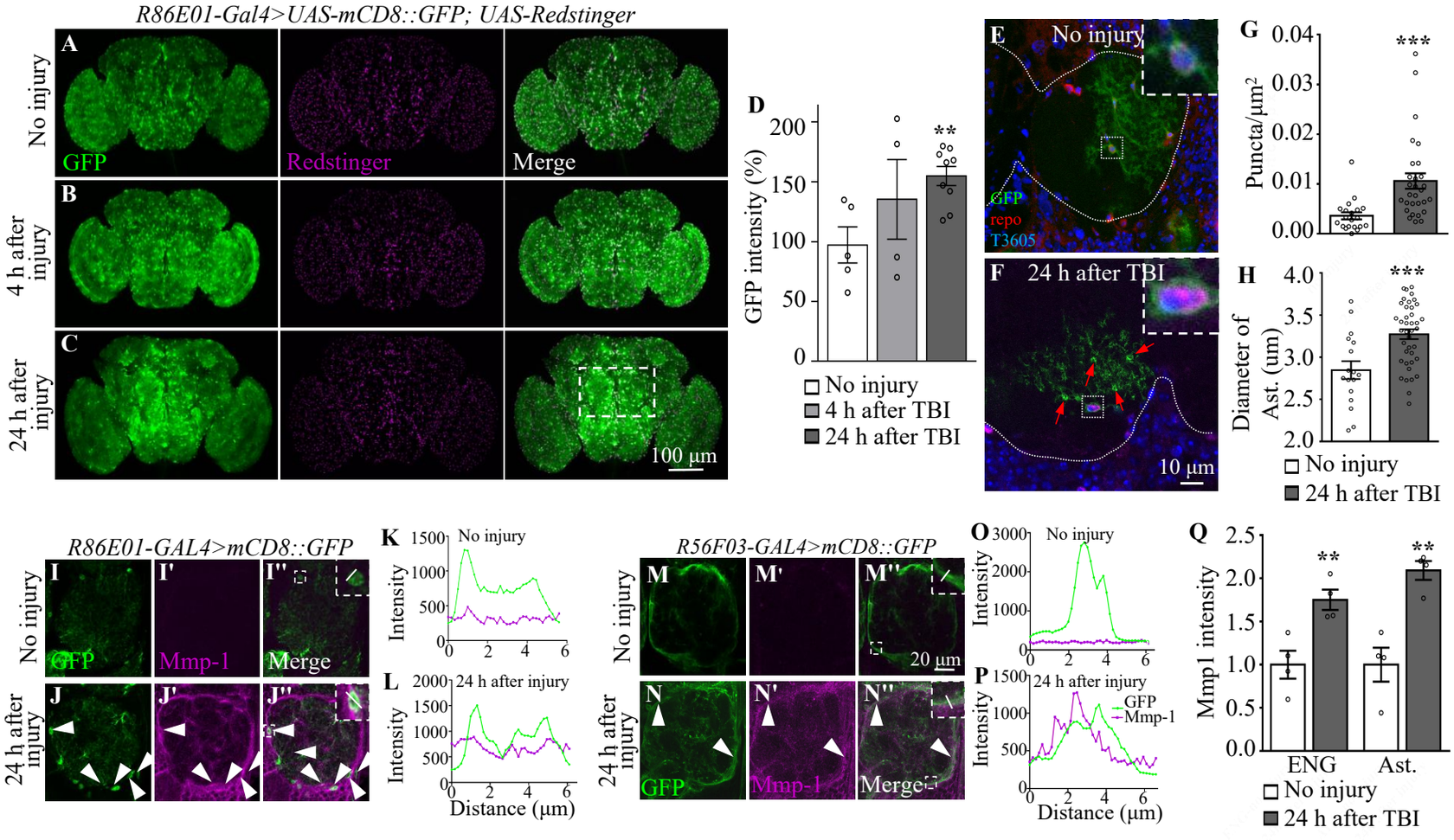
R86E01-Gal4>UAS-mCD8::GFP; UAS-Redstinger
A
B
C
No injury
4 h after injury
24 h after injury
GFP
Redstinger
Merge
100 µm
D
GFP intensity (%)
No injury
4 h after TBI
24 h after TBI
E
No injury
GFP
repo
T3605
F
24 h after TBI
10 µm
G
Puncta/µm²
H
Diameter of Ast. (um)
R86E01-GAL4>mCD8::GFP
I
I'
I''
J
J'
J''
Mmp-1
K
L
Intensity
Distance (µm)
R56F03-GAL4>mCD8::GFP
M
M'
M''
N
N'
N''
20 µm
O
P
GFP
Mmp-1
Q
Mmp1 intensity
ENG
Ast.

Figure 3

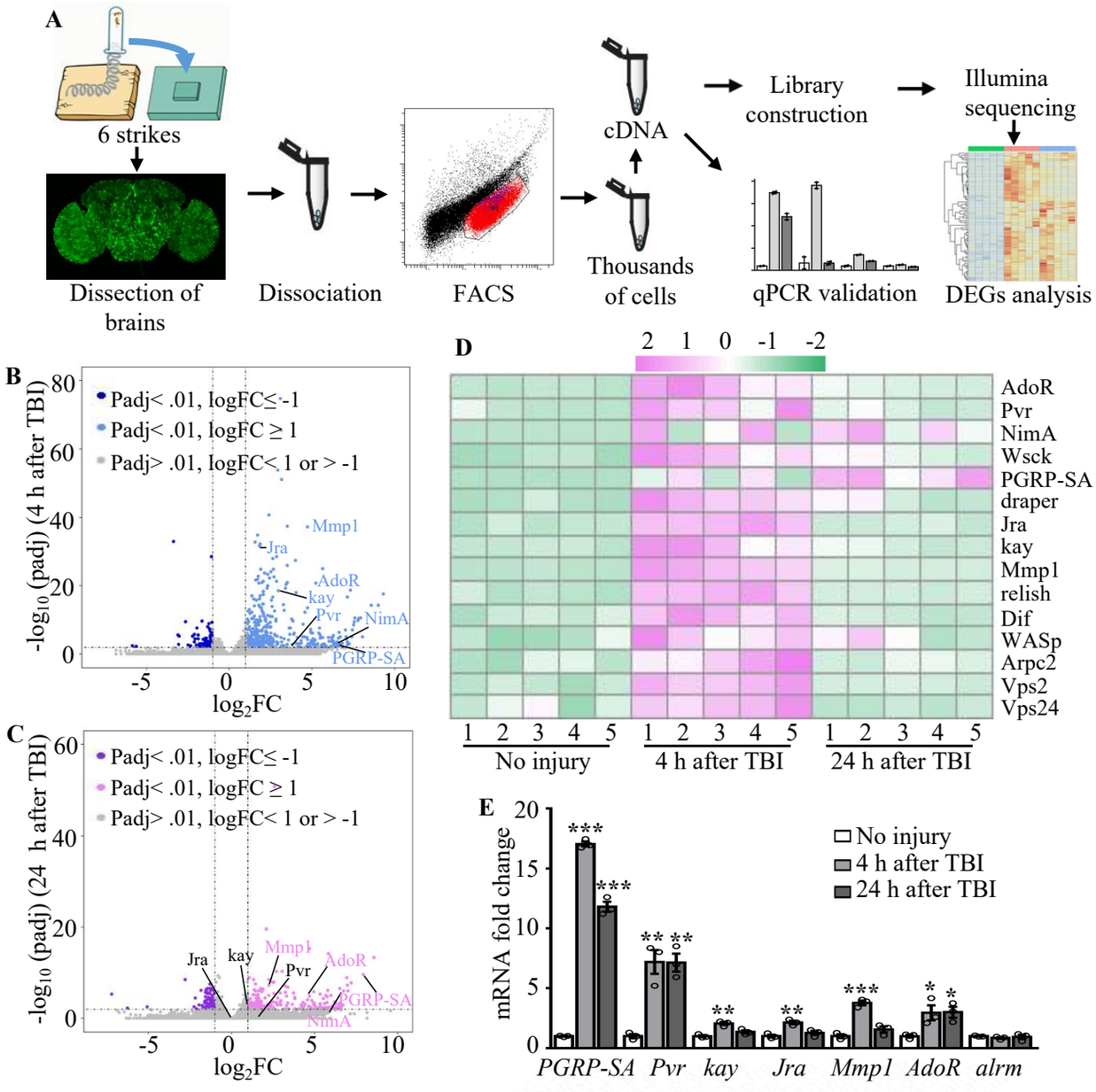
A
6 strikes
Dissection of brains
Dissociation
FACS
Thousands of cells
cDNA
Library construction
Illumina sequencing
qPCR validation
DEGs analysis
B
Padj< .01, logFC≤ -1
Padj< .01, logFC ≥ 1
Padj> .01, logFC< 1 or > -1
-log10 (padj) (4 h after TBI)
log2FC
Mmp1
Jra
AdoR
kay
Pvr
NimA
PGRP-SA
C
Padj< .01, logFC≤ -1
Padj< .01, logFC ≥ 1
Padj> .01, logFC< 1 or > -1
-log10 (padj) (24 h after TBI)
log2FC
Jra
kay
Mmp1
Pvr
AdoR
PGRP-SA
NimA
D
2 1 0 -1 -2
AdoR
Pvr
NimA
Wsck
PGRP-SA
draper
Jra
kay
Mmp1
relish
Dif
WASp
Arpc2
Vps2
Vps24
No injury
4 h after TBI
24 h after TBI
E
mRNA fold change
No injury
4 h after TBI
24 h after TBI
PGRP-SA
Pvr
kay
Jra
Mmp1
AdoR
alrm

Table 1

Genes in *Drosophila*	Conserved genes in mouse	Conserved genes in human	4 h after injury (FC)	24 h after injury (FC)
Pvr	pdgfr/vegfr	VEGFR	13.83	2.79
AdoR	Adora2a	ADORA2B	37.53	7.73
Mmp1	Mmp14	MMP14	26.35	4.79
Jra	Jun	JUN	3.58	1.18
kay	FOSL2	FOS	6.23	1.77
cpa	Capza2	CAPZA1	3.43	1.72
cpb	Capzb	CAPZB	2.01	1.25
Stam	Stam2	STAM	2.14	1.46
Chmp1	Chmp1b	CHMP1B	2.16	0.92
Vps24	Chmp3	CHMP3	2.11	0.87

Figure 4

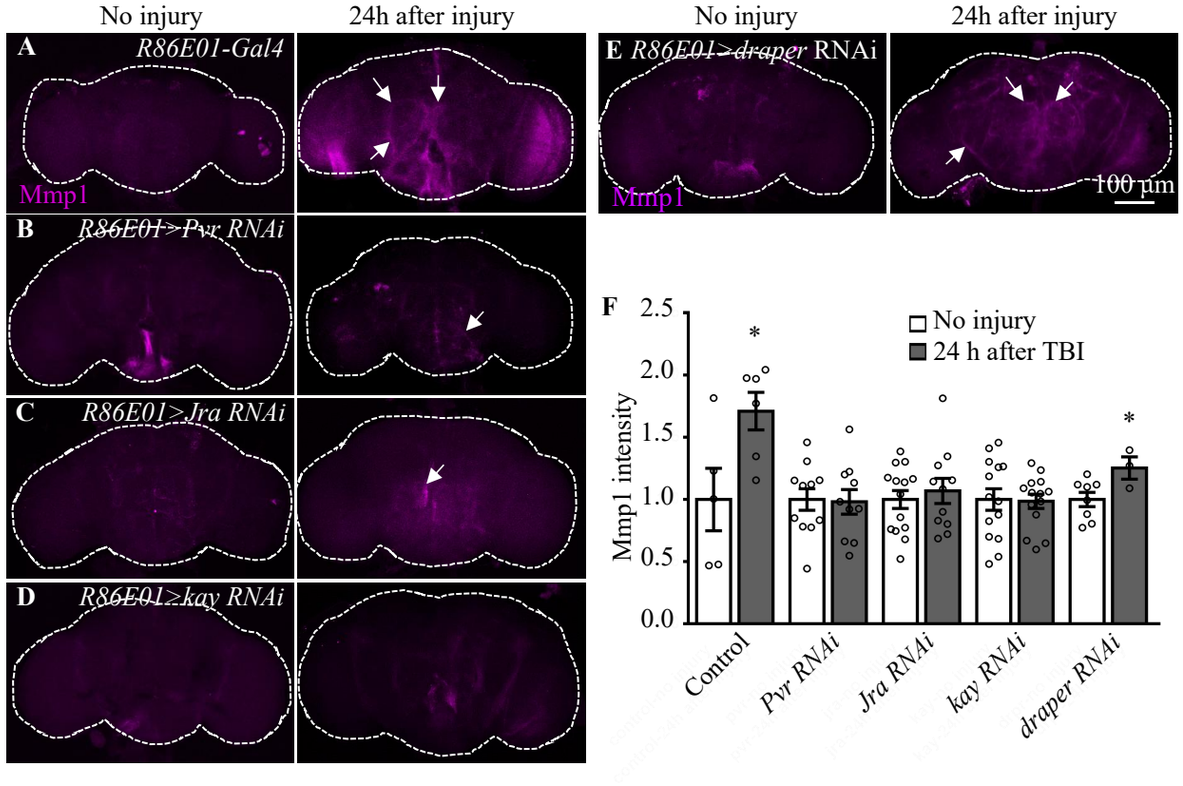
No injury
24h after injury
A R86E01-Gal4
Mmp1
B R86E01>Pvr RNAi
C R86E01>Jra RNAi
D R86E01>kay RNAi
No injury
24h after injury
E R86E01>draper RNAi
Mmp1
100 µm
F
No injury
24 h after TBI
Mmp1 intensity
2.5
2.0
1.5
1.0
0.5
0.0
*
*
Control
Pvr RNAi
Jra RNAi
kay RNAi
draper RNAi

Figure 5

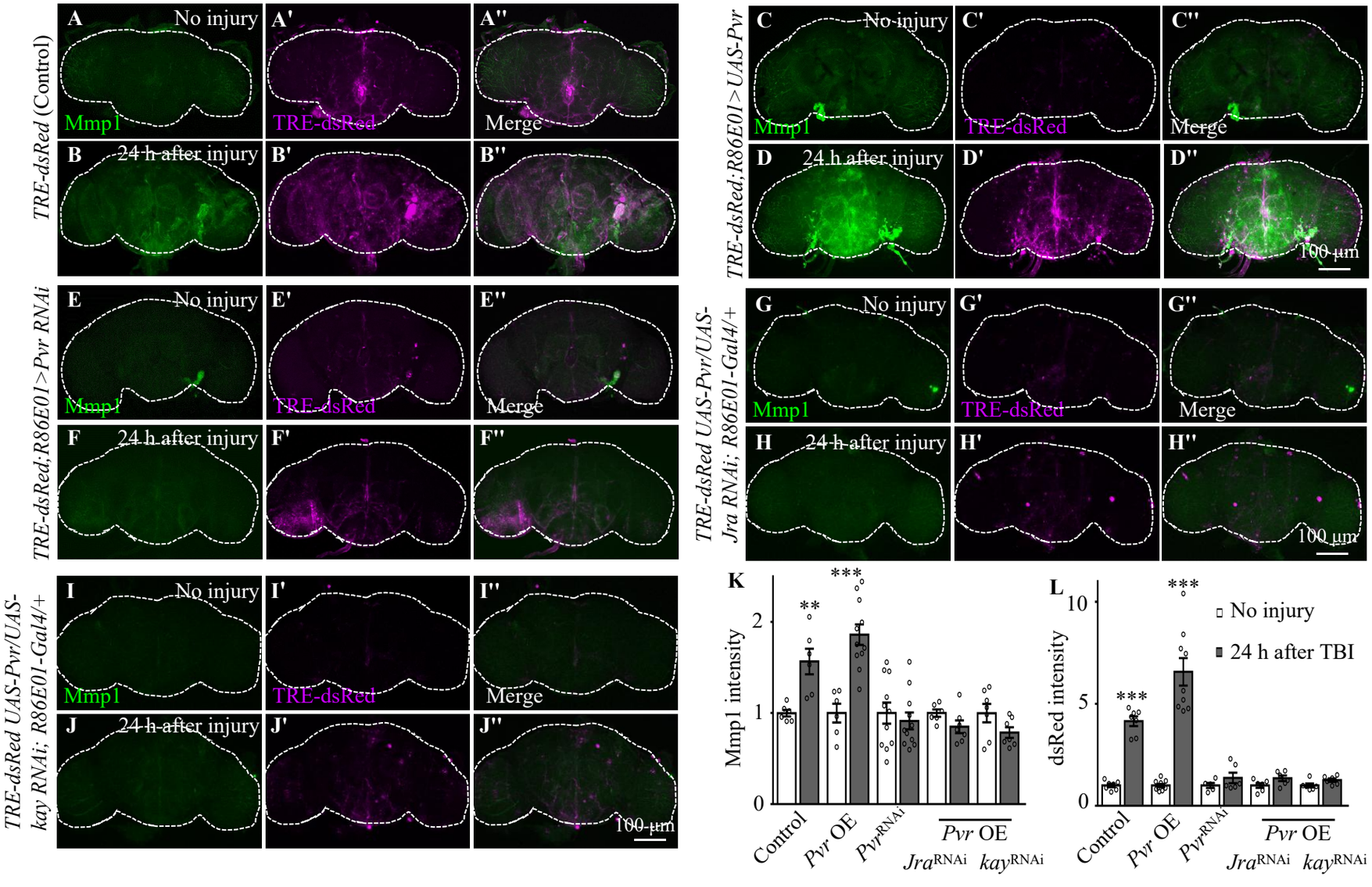
TRE-dsRed (Control)
TRE-dsRed;R86E01>Pvr RNAi
TRE-dsRed UAS-Pvr/UAS-kay RNAi; R86E01-Gal4/+
TRE-dsRed;R86E01>UAS-Pvr
TRE-dsRed UAS-Pvr/UAS-Jra RNAi; R86E01-Gal4/+
A No injury
A'
A''
B 24 h after injury
B'
B''
C No injury
C'
C''
D 24 h after injury
D'
D''
E No injury
E'
E''
F 24 h after injury
F'
F''
G No injury
G'
G''
H 24 h after injury
H'
H''
I No injury
I'
I''
J 24 h after injury
J'
J''
Mmp1
TRE-dsRed
Merge
100 µm
K
Mmp1 intensity
No injury
24 h after TBI
Control
Pvr OE
Pvr^RNAi
Pvr OE
Jra^RNAi
kay^RNAi
L
dsRed intensity

Figure 6

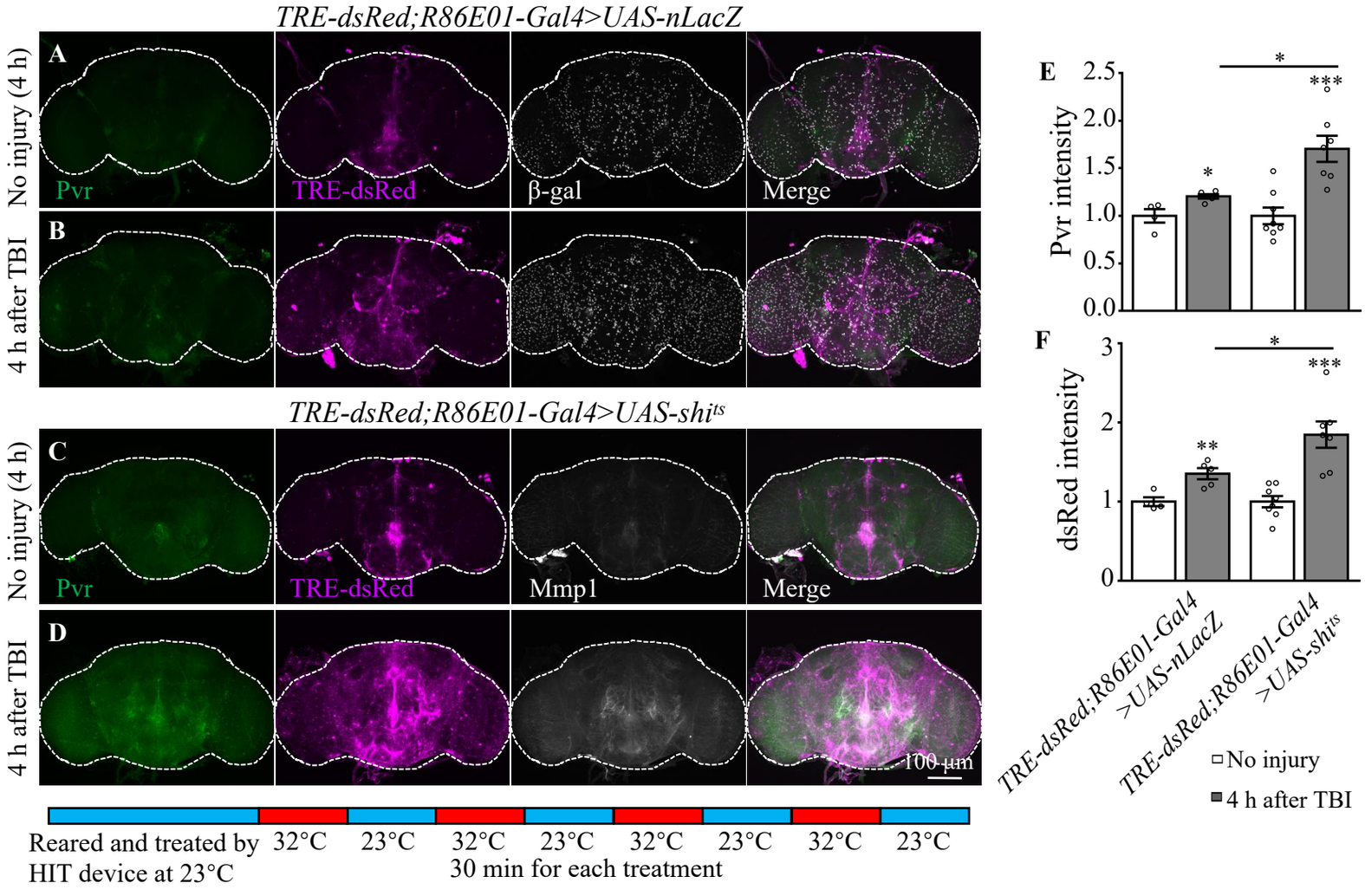
TRE-dsRed;R86E01-Gal4>UAS-nLacZ
A
B
No injury (4 h)
4 h after TBI
Pvr
TRE-dsRed
β-gal
Merge
TRE-dsRed;R86E01-Gal4>UAS-shi^ts
C
D
Mmp1
100 μm
Reared and treated by HIT device at 23°C
32°C
23°C
30 min for each treatment
E
F
Pvr intensity
dsRed intensity
TRE-dsRed;R86E01-Gal4 >UAS-nLacZ
TRE-dsRed;R86E01-Gal4 >UAS-shi^ts
No injury
4 h after TBI

Figure 7

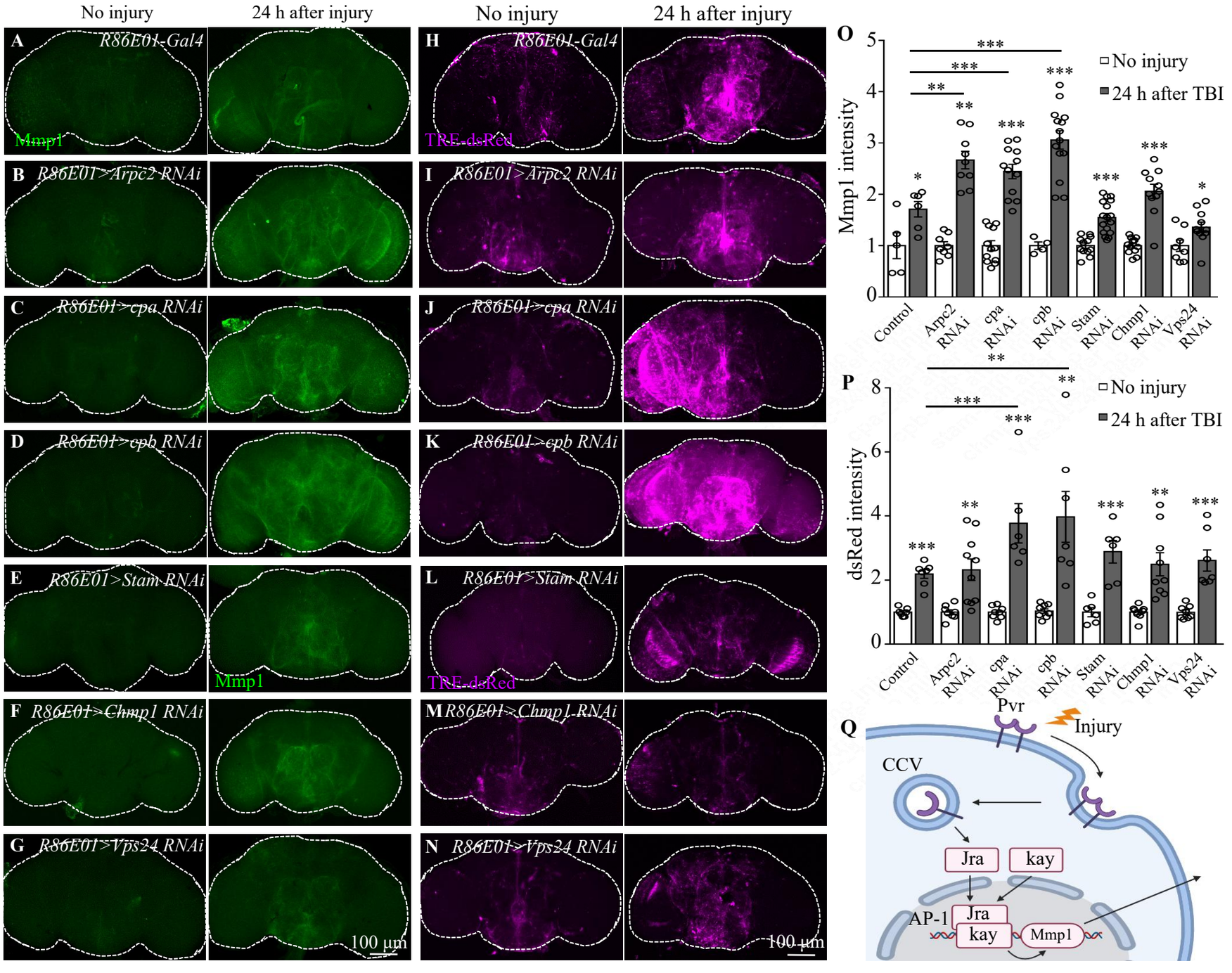
No injury
24 h after injury
No injury
24 h after injury
A R86E01-Gal4
Mmp1
B R86E01>Arpc2 RNAi
C R86E01>cpa RNAi
D R86E01>cpb RNAi
E R86E01>Stam RNAi
Mmp1
F R86E01>Chmp1 RNAi
G R86E01>Vps24 RNAi
100 μm
H R86E01-Gal4
TRE-dsRed
I R86E01>Arpc2 RNAi
J R86E01>cpa RNAi
K R86E01>cpb RNAi
L R86E01>Stam RNAi
TRE-dsRed
M R86E01>Chmp1 RNAi
N R86E01>Vps24 RNAi
100 μm
O
Mmp1 intensity
No injury
24 h after TBI
Control
Arpc2 RNAi
cpa RNAi
cpb RNAi
Stam RNAi
Chmp1 RNAi
Vps24 RNAi
P
dsRed intensity
No injury
24 h after TBI
Control
Arpc2 RNAi
cpa RNAi
cpb RNAi
Stam RNAi
Chmp1 RNAi
Vps24 RNAi
Q
Pvr
Injury
CCV
Jra
kay
AP-1
Jra
kay
Mmp1

Figure S1

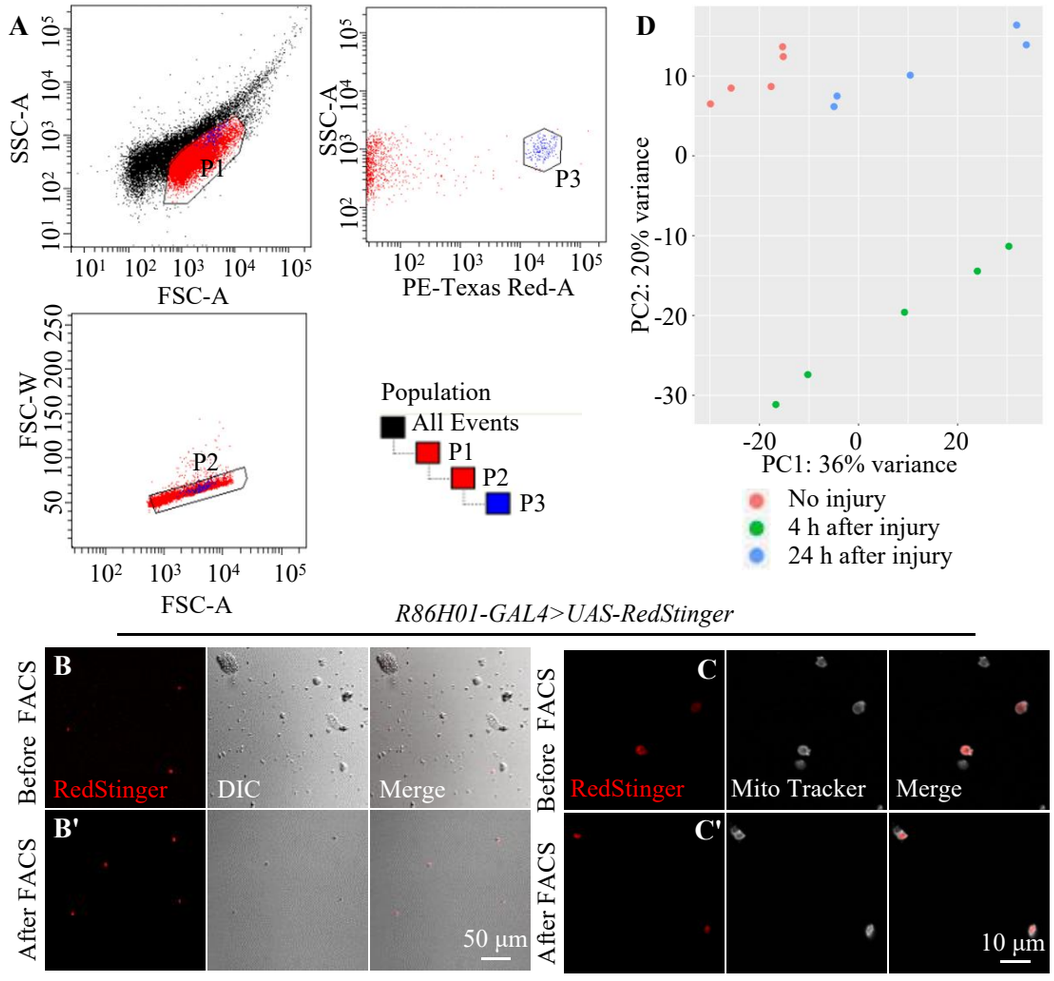
A
SSC-A
FSC-A
P1
SSC-A
PE-Texas Red-A
P3
FSC-W
FSC-A
P2
Population
All Events
P1
P2
P3
D
PC2: 20% variance
PC1: 36% variance
No injury
4 h after injury
24 h after injury
R86H01-GAL4>UAS-RedStinger
Before FACS
After FACS
B
RedStinger
DIC
Merge
B'
50 µm
C
RedStinger
Mito Tracker
Merge
C'
10 µm

Figure S2

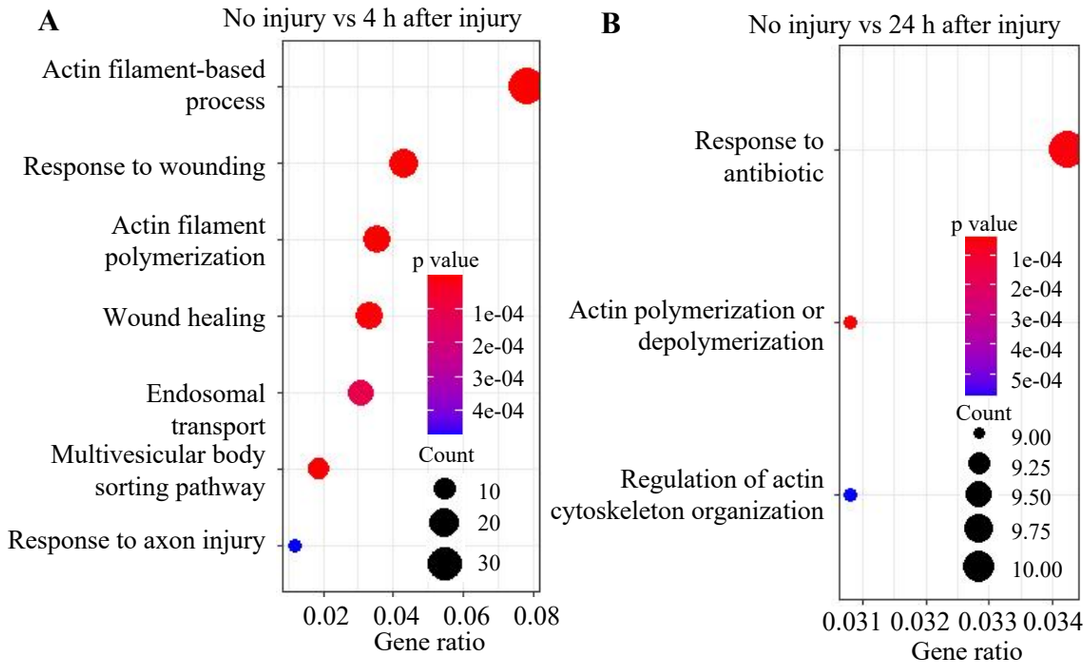
A
No injury vs 4 h after injury
Actin filament-based process
Response to wounding
Actin filament polymerization
Wound healing
Endosomal transport
Multivesicular body sorting pathway
Response to axon injury
p value
1e-04
2e-04
3e-04
4e-04
Count
10
20
30
0.02
0.04
0.06
0.08
Gene ratio
B
No injury vs 24 h after injury
Response to antibiotic
Actin polymerization or depolymerization
Regulation of actin cytoskeleton organization
p value
1e-04
2e-04
3e-04
4e-04
5e-04
Count
9.00
9.25
9.50
9.75
10.00
0.031
0.032
0.033
0.034
Gene ratio

Figure S3

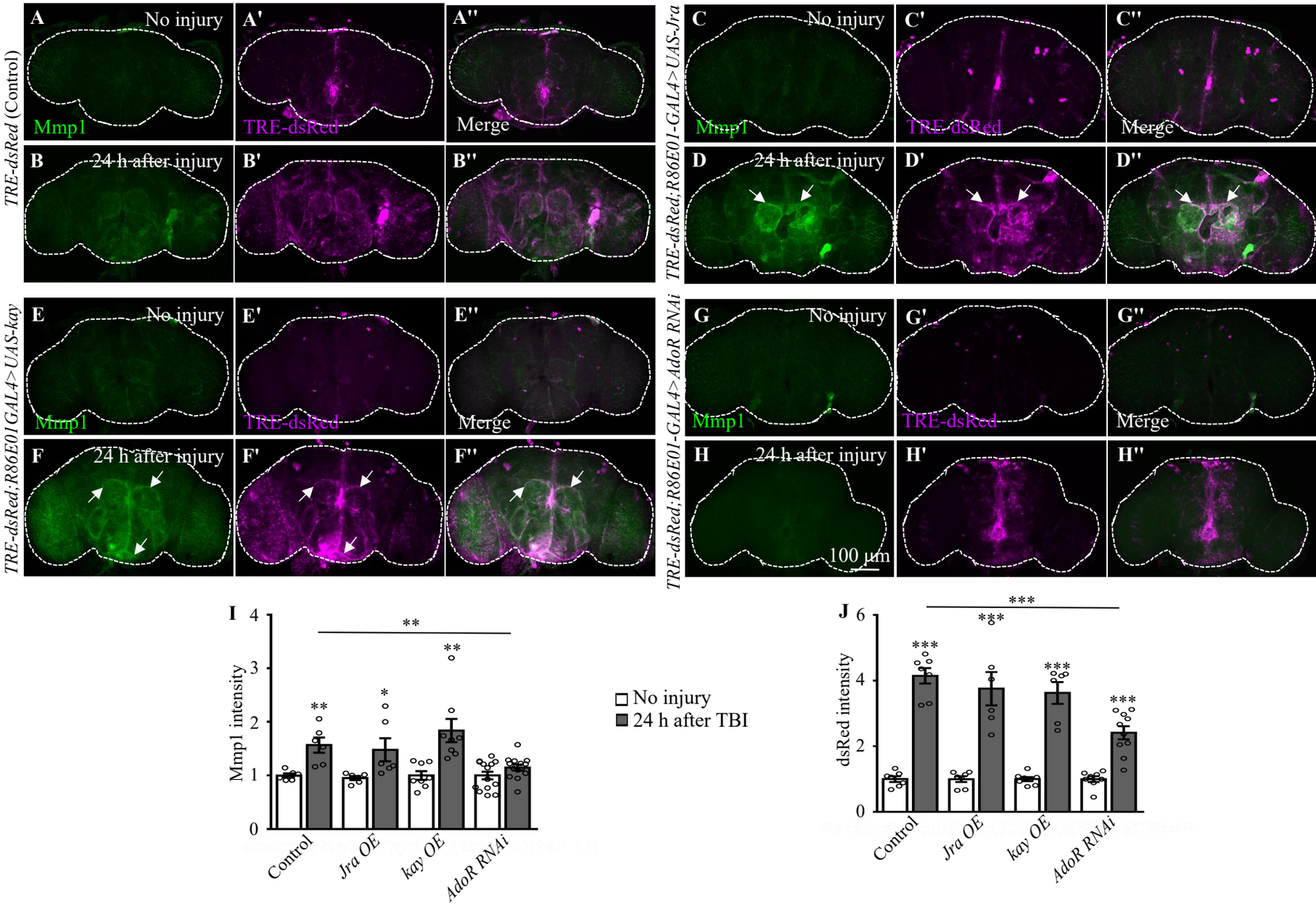
TRE-dsRed (Control)
TRE-dsRed;R86E01-GAL4>UAS-Jra
TRE-dsRed;R86E01-GAL4>UAS-kay
TRE-dsRed;R86E01-GAL4>AdoR RNAi
A No injury
A'
A''
Mmp1
TRE-dsRed
Merge
B 24 h after injury
B'
B''
C No injury
C'
C''
D 24 h after injury
D'
D''
E No injury
E'
E''
F 24 h after injury
F'
F''
G No injury
G'
G''
H 24 h after injury
H'
H''
100 μm
I
Mmp1 intensity
No injury
24 h after TBI
Control
Jra OE
kay OE
AdoR RNAi
J
dsRed intensity